4. Experimental

4.1. Cell cultures

MKN45[15] and HCT116[17] cancer cell lines, together with those transfected with GnT-V[15] and GMDS[17] were established and cultured as described previously.

4.2. Mice preparation and noninvasive fluorescence imaging

Seven week-old mice (BALB/cAJcl–nu/nu, CLEA Japan, Inc.) were used for in vivo fluorescence imaging. Fluorescence-labeled cancer cell lines (1×10^6 cells/100 μL in HBSS buffer) were administered into the abdominal cavity without anesthesia, and whole body scan was performed by using eXplore Optix apparatus, GE Healthcare, Bioscience, over 35 days after injection (excitation at 730 nm, emission 750 nm).[18] The in vivo fluorescence image was taken under inhalation anesthesia with Isoflurane®; the concentration of Isoflurane® was kept at 1.5–2% during the measurements. After the whole-body imaging, the mice were painlessly sacrificed under anesthesia and the fluorescence in each organ, that is, heart, lung, stomach, liver, kidney, spleen, pancreas, and colon, was measured by eXplore Optix, GE Healthcare, Bioscience (excitation at 730 nm, emission 750 nm).

Acknowledgments

This work was supported in part by Grants-in-Aid for Scientific Research No. 23681047 from the Japan Society for the Promotion of Science and the 'Hisyo-30' program for young investigators from Osaka University.

Supplementary data

Supplementary data associated with this article can be found, in the online version, at http://dx.doi.org/10.1016/j.bmc.2013.01.005.

References and notes

1. Representative examples for cell trafficking and metastasis imaging; see, (a) Sutton, E. J.; Henning, T. D.; Pichler, B. J.; Bremer, C.; Daldrup-Link, H. E. *Eur. Radiol.* **2008**, *18*, 2021; (b) Kaichenko, V.; Neeman, M.; Harmelin, A. *Springer Ser. Fluoresc.* **2011**, *10*, 329; (c) Seitz, G.; Warmann, S. W.; Fuchs, J.; Heitmann, H.; Mahrt, J.; Busse, A.-C.; Ruck, P.; Hoffman, R. M.; Wessels, J. T. *Cell Prolif.* **2008**, *41*, 365; (d) Zal, T.; Chodaczek, G. *Semin. Immunopathol.* **2010**, *32*, 305.
2. Ottobrini, L.; Martelli, C.; Trabattoni, D. L.; Clerici, M.; Lucignani, G. *Eur. J. Nucl. Med. Mol. Imaging* **2011**, *38*, 949.
3. Baxevanis, C. N.; Papamichail, M. *Cancer Immunol. Immunother.* **2004**, *53*, 893.
4. (a) Zhao, C.; Tian, M.; Zhang, H. *Open Nucl. Med. J.* **2010**, *2*, 171; (b) Lee, Z.; Dennis, J. E.; Gerson, S. L. *Exp. Biol. Med.* **2008**, *233*, 930; (c) Reagan, M. R.; Kaplan, D. L. *Stem Cells* **2011**, *29*, 920; (d) Tsurumi, C.; Esser, N.; Firat, E.; Gaedicke, S.; Follo, M.; Behe, M.; Elsässer-Beile, U.; Grosu, A.-L.; Graeser, R.; Niedermann, G. *PLoS One* **2010**, *5*, e15605.
5. Leading reviews of cell trafficking PET, see: (a) Oku, N.; Asai, T. *Lung Biol. Health Dis.* **2005**, *203*, 349; (b) Levin, C. S. *Proc. IEEE* **2008**, *96*, 439.
6. Representative examples of MRI using the whole cells, see: (a) Yeh, T.-C.; Zhang, W.; Ildstad, S. T.; Ho, C. *Magn. Reson. Med.* **1993**, *30*, 617; (b) Bulte, J. W. M.; Duncan, I. D.; Frank, J. A. *J. Cereb. Blood Flow Metab.* **2002**, *22*, 899; (c) Hoehn, M.; Kustermann, E.; Blunk, J.; Wiedermann, D.; Trapp, T.; Wecker, S.; Focking, M.; Arnold, H.; Hescheler, J.; Fleischmann, B. K.; Schwindt, W.; Buhrle, C. *Proc. Natl. Acad. Sci. U.S.A.* **2002**, *99*, 16267; (d) Toyoda, K.-I.; Tooyama, I.; Kato, M.; Sato, H.; Morikawa, S.; Hisa, Y.; Inubushi, T. *Neuroreport* **2004**, *15*, 589.
7. (a) Saxon, E.; Bertozzi, C. R. *Science* **2000**, *287*, 2007; (b) Kiick, K. L.; Saxon, E.; Tirrell, D. A.; Bertozzi, C. R. *Proc. Natl. Acad. Sci. U.S.A.* **2002**, *99*, 19; (c) Vocadlo, D. J.; Hang, H. C.; Kim, E. J.; Hanover, J. A.; Bertozzi, C. R. *Proc. Natl. Acad. Sci. U.S.A.* **2003**, *100*, 9116; (d) Paulick, M. G.; Forstner, M. B.; Groves, J. T.; Bertozzi, C. R. *Proc. Natl. Acad. Sci. U.S.A.* **2007**, *104*, 20332.
8. Luchansky, S. J.; Bertozzi, C. R. *ChemBioChem* **2004**, *5*, 1706; (b) Agard, N. J.; Baskin, J. M.; Prescher, J. A.; Lo, A.; Bertozzi, C. R. *ACS Chem. Biol.* **2006**, *1*, 644; (c) Prescher, J. A.; Bertozzi, C. R. *Cell* **2006**, *126*, 851; (d) Baskin, J. M.; Prescher, J. A.; Laughlin, S. T.; Agard, N. J.; Chang, P. V.; Miller, I. A.; Lo, A.; Codelli, J. A.; Bertozzi, C. R. *Proc. Natl. Acad. Sci. U.S.A.* **2007**, *104*, 16793; (e) Fernandez-Suarez, M.; Baruah, H.; Martinez-Hernandez, L.; Xie, K. T.; Baskin, J. M.; Bertozzi, C. R.; Ting, A. Y. *Nat. Biotechnol.* **2007**, *25*, 1483; (f) Ning, X.; Guo, J.; Wolfert, M. A.; Boons, G.-J. *Angew. Chem., Int. Ed.* **2008**, *47*, 2253; (g) Sanders, B. C.; Friscourt, F.; Ledin, P. A.; Mbua, N. E.; Arumugam, S.; Guo, J.; Boltje, T. J.; Popik, V. V.; Boons, G.-J. *J. Am. Chem. Soc.* **2011**, *133*, 949; (h) Kii, I.; Shiraishi, A.; Hiramatsu, T.; Matsushima, T.; Uekusa, H.; Yoshida, S.; Yamamoto, M.; Kudo, A.; Hagiwara, M.; Hosoya, T. *Org. Biomol. Chem.* **2010**, *8*, 4051.
9. Spicer, C. D.; Triemer, T.; Davis, B. G. *J. Am. Chem. Soc.* **2012**, *134*, 800.
10. (a) Laughlin, S. T.; Baskin, J. M.; Amacher, S. L.; Bertozzi, C. R. *Science* **2008**, *320*, 664; (b) Laughlin, S. T.; Bertozzi, C. R. *ACS Chem. Biol.* **2009**, *4*, 1068; (c) Chang, P. V.; Prescher, J. A.; Sletten, E. M.; Baskin, J. M.; Miller, I. A.; Agard, N. J.; Lo, A.; Bertozzi, C. R. *Proc. Natl. Acad. Sci. U.S.A.* **2010**, *107*, 1821.
11. (a) Tanaka, K.; Kamatani, M.; Mori, H.; Fujii, S.; Ikeda, K.; Hisada, M.; Itagaki, Y.; Katsumura, S. *Tetrahedron* **1999**, *55*, 1657; (b) Tanaka, K.; Mori, H.; Yamamoto, M.; Katsumura, S. *J. Org. Chem.* **2001**, *66*, 3099; (c) Tanaka, K.; Katsumura, S. *J. Am. Chem. Soc.* **2002**, *124*, 9660; (d) Tanaka, K.; Kobayashi, T.; Mori, H.; Katsumura, S. *J. Org. Chem.* **2004**, *69*, 5906.
12. (a) Tanaka, K.; Masuyama, T.; Hasegawa, K.; Tahara, T.; Mizuma, H.; Wada, Y.; Watanabe, Y.; Fukase, K. *Angew. Chem., Int. Ed.* **2008**, *47*, 102; (b) Tanaka, K.; Fukase, K. *Org. Biomol. Chem.* **2008**, *6*, 815; (c) Tanaka, K.; Siwu, E. R. O.; Minami, K.; Hasegawa, K.; Nozaki, S.; Kanayama, Y.; Koyama, K.; Chen, C. W.; Paulson, J. C.; Watanabe, Y.; Fukase, K. *Angew. Chem., Int. Ed.* **2010**, *49*, 8195; (d) Tanaka, K.; Fukase, K.; Katsumura, S. *Chem. Rec.* **2010**, *10*, 119; (e) Tanaka, K.; Fukase, K.; Katsumura, S. *Synlett* **2011**, 2115.
13. (a) Tanaka, K.; Minami, K.; Tahara, T.; Fujii, Y.; Siwu, E. R. O.; Nozaki, S.; Onoe, H.; Yokoi, S.; Koyama, K.; Watanabe, Y.; Fukase, K. *Chem. Med. Chem.* **2010**, *5*, 841; (b) Tanaka, K.; Yokoi, S.; Morimoto, K.; Iwata, T.; Nakamoto, Y.; Nakayama, K.; Koyama, K.; Fujiwara, T.; Fukase, K. *Bioorg. Med. Chem.* **2012**, *20*, 1865.
14. Tanaka, K.; Minami, K.; Tahara, T.; Siwu, E. R. O.; Koyama, K.; Nozaki, S.; Onoe, H.; Watanabe, Y.; Fukase, K. J. *Carbohydr. Chem.* **2010**, *29*, 118.
15. Ihara, S.; Miyoshi, E.; Ko, J. H.; Murata, K.; Nakahara, S.; Honke, K.; Dickson, R. B.; Lin, C.-Y.; Taniguchi, N. *J. Biol. Chem.* **2002**, *277*, 16960.
16. Lau, K. S.; Dennis, J. W. *Glycobiology* **2008**, *18*, 750.
17. (a) Moriwaki, K.; Noda, K.; Furukawa, Y.; Ohshima, K.; Uchiyama, A.; Nakagawa, T.; Taniguchi, N.; Daigo, Y.; Nakamura, Y.; Hayashi, N.; Miyoshi, E. *Gastroenterology* **2009**, *137*, 188; (b) Moriwaki, K.; Shinzaki, S.; Miyoshi, E. *J. Biol. Chem.* **2011**, *286*, 43123.
18. Hirai, M.; Minematsu, H.; Kondo, N.; Oie, K.; Igarashi, K.; Yamazaki, N. *Biochem. Biophys. Res. Commun.* **2007**, *353*, 553.

Carbohydrate Research 374 (2013) 49–58

Contents lists available at SciVerse ScienceDirect

Carbohydrate Research

journal homepage: www.elsevier.com/locate/carres

Preparation of branched cyclomaltoheptaose with 3-*O*-α-L-fucopyranosyl-α-D-mannopyranose and changes in fucosylation of HCT116 cells treated with the fucose-modified cyclomaltoheptaose

Madoka Kimura [a], Yuki Masui [a], Yuko Shirai [a], Chie Honda [a], Kenta Moriwaki [b], Taku Imai [b], Uichiro Takagi [d], Takaaki Kiryu [c], Taro Kiso [c], Hiromi Murakami [c], Hirofumi Nakano [c], Sumio Kitahata [d], Eiji Miyoshi [b], Toshiko Tanimoto [a,*]

[a] *School of Pharmaceutical Sciences, Mukogawa Women's University, Nishinomiya, Japan*
[b] *Osaka University Graduate School of Medicine, Suita, Japan*
[c] *Osaka Municipal Technical Research Institute, Osaka, Japan*
[d] *Department of Bioscience and Biotechnology, Shinshu University, Nagano, Japan*

ARTICLE INFO

Article history:
Received 31 January 2013
Received in revised form 23 March 2013
Accepted 23 March 2013
Available online 3 April 2013

Keywords:
α-Fucosidase
6^{I},6^{IV}-Di-*O*-(3-*O*-α-L-fucopyranosyl-α-D-mannopyranosyl)-cyclomaltoheptaose
HCT116 cells

ABSTRACT

From a mixture of 4-nitrophenyl α-L-fucopyranoside and D-mannopyranose, 3-*O*-α-L-fucopyranosyl-D-mannopyranose was synthesised through the transferring action of α-fucosidase (Sumizyme PHY). 6^{I},6^{IV}-Di-*O*-(3-*O*-α-L-fucopyranosyl-α-D-mannopyranosyl)-cyclomaltoheptaose {**8**, 6^{I},6^{IV}-di-*O*-[α-L-Fuc-(1→3)-α-D-Man]-βCD} was chemically synthesised using the trichloroacetimidate method. The structures were confirmed by MS and NMR spectroscopy. A cell-based assay using the fucosyl βCD derivatives, including the newly synthesised **8**, showed that derivatives with two branches of the α-L-Fuc or α-L-Fuc-(1→3)-α-D-Man residues possessed slight growth-promoting effects and lower toxicity in HCT116 cells compared to those with one branch. These compounds may be useful as drug carriers in targeted drug delivery systems.

1. Introduction

Branched cyclomaltooligosaccharides (CDs) having mono- or oligosaccharides linked to hydroxyl groups on the C-6 carbons of the CDs are potentially useful drug carriers for targeted drug delivery systems.[1–3] CDs have the ability to form inclusion complexes by incorporating various hydrophobic compounds into their interior cavities.[4] We have attempted to synthesise various homogeneous and heterogeneous branched CDs via chemical synthesis[5–9] and enzymatic reactions.[10–14] In particular, the positional isomers of di-branched glycosyl CDs, as described by the glycoside cluster effect,[15,16] are thought to possess characteristic abilities for molecular recognition arising from differences in the positions of their substituents. The water solubility of branched cyclomaltoheptaoses (βCDs) linked with mono- or oligosaccharides containing glucose, galactose, mannose and maltose is approximately 50–100 times that of βCD.[17,18] Therefore, the use of branched βCD inclusion complexes is expected to increase the bioavailability of insoluble and unstable drugs.

L-Fucose (L-Fuc), a deoxyhexose, is a biologically important monosaccharide. For example, α-L-Fuc residues in the carbohydrate chains of glycoconjugates act as cell–cell recognition sites and as important antigenic determinants such as blood group antigens.[19–21] Fucosylation is one of the most important oligosaccharide modifications in cancer. Fucosylation is catalysed by several types of fucosyltransferases, which require guanosine diphosphate (GDP)-fucose as a donor substrate. Most GDP-fucose is synthesised by a de novo pathway in which GDP-mannose is transformed by GDP-mannose-4,6-dehydratase (GMDS). Free α-L-Fuc is converted to GDP-fucose through the salvage pathway, which is a minor pathway. We recently found a virtually complete deficiency of fucosylation resulting from an alteration of GMDS transcripts in a human colon cancer cell line, HCT116, that escaped the immune surveillance system.[22] HCT116 cells express abnormal GMDS mRNA that leads to inactivation of the de novo pathway for GDP-fucose synthesis followed by cellular fucosylation deficiency.

We recently reported the chemical synthesis of branched CDs in which two L-Fuc residues were linked to βCD through an α-(1→6)-linkage, resulting in 6^{I},6^{n}-di-*O*-(α-L-fucopyranosyl)-βCDs [6^{I},6^{n}-di-*O*-(α-L-Fuc)-βCDs, *n* = II–IV].[23] The molecular interaction between these compounds and the fucose-binding lectin *Aleuria aurantia* lectin (AAL) was investigated using an optical biosensor based on

* Corresponding author. Tel.: +81 798 45 9950.
E-mail address: tanimoto@mukogawa-u.ac (T. Tanimoto).

0008-6215/$ - see front matter © 2013 Elsevier Ltd. All rights reserved.
http://dx.doi.org/10.1016/j.carres.2013.03.022

a surface plasmon resonance (SPR) technique. The order of binding affinity, as a function of the fucose-binding position, was $6^{I},6^{IV}$- > $6^{I},6^{III}$- > $6^{I},6^{II}$-di-*O*-(α-L-Fuc)-βCD > 6-*O*-(α-L-Fuc)-βCD.

We hypothesised that the length of the sugar side chains attached to the CD ring leads to differences in the functions of the branched CDs. D-Mannose was a more convenient monosaccharide to synthesise the disaccharide with α-L-fucose residue by enzyme-catalysed reactions using α-fucosidase (unpublished data). The α-D-mannose residue has been observed in many glycolipids and glycoproteins on the cell surface. Furthermore we examined glycosylation using the trichloroacetimidate method in order to synthesise branched CDs.[24] Mannosylation in the presence of trifluoromethanesulfonic acid or trimethylsilyl trifluoromethanesulfonate as a catalyst gave only the α-mannoside CD. This was a very important result, because it showed that this could be used easily for purification.

In this study, 3-*O*-α-L-fucopyranosyl-D-mannopyranose [α-L-Fuc-(1→3)-D-Man] was synthesised through the transfer action of α-fucosidase (Sumizyme PHY) from a 4-nitrophenyl α-L-fucopyranoside and D-Man. $6^{I},6^{IV}$-Di-*O*-(3-*O*-α-L-fucopyranosyl-α-D-mannopyranosyl)-cyclomaltoheptaose {**8**, $6^{I},6^{IV}$-di-*O*-[α-L-Fuc-(1→3)-α-D-Man]-βCD} was chemically synthesised using the trichloroacetimidate method (Chart 1). The applicability of this compound as a drug carrier for targeted drug delivery systems was evaluated through investigation of cell toxicity in a colon cancer cell line, HCT116.

2. Results and discussion

2.1. Enzymatic synthesis of α-L-fucopyranosyl-D-mannopyranose (α-L-Fuc-D-Man) by transglycosylation of α-fucosidase (Sumizyme PHY)

2.1.1. Partial purification of α-fucosidase

Sumizyme PHY (19.4 g) was suspended in water (116 mL) (**I**), and the suspension was added to 4.6 M ammonium sulphate (506 mL). After standing overnight at 4 °C, the supernatant (**II**) and the precipitates were separated by centrifugation, and the precipitates were dissolved in 20 mM sodium acetate buffer (**III**) (29 mL).

2.1.2. Enzyme assay[25,26]

Ten microlitres of each enzyme solution (**I**, **II** and **III**) was incubated with 40 μL of 10 mM 4-nitrophenyl α-L-fucopyranoside in 40 μL of 0.2 M sodium acetate buffer (pH 4.0) for 10 min at 40 °C. The reaction was stopped by adding 100 μL of a 0.2 M Na_2CO_3 solution, and the release of 4-nitrophenol was measured spectrophotometrically at 400 nm. One unit of enzyme activity was defined as the amount of enzyme able to release 1 μmol of 4-nitrophenol per min. Then, the concentration of protein in 10 μL of each enzyme solution (**I**, **II** and **III**) diluted in 40 μL of 0.2 M sodium acetate buffer (pH 4.0) was also measured spectrophotometrically at 280 nm. The specific activity of solution **III** was the highest, and it was used in the following experiments without further purification (Table 1).

2.1.3. Effects of enzyme concentration on the formation of α-L-fucopyranosyl-D-mannopyranose (α-L-Fuc-D-Man)

Reaction mixtures containing D-Man and 4-nitrophenyl α-L-fucopyranoside in sodium acetate buffer (pH 4.0) were incubated at 40 °C for 28 h with solution **III** and varying concentrations of enzyme, (A) 0.118 U/mL of α-fucosidase, (B) 0.300 U/mL of α-fucosidase and (C) 0.500 U/mL of α-fucosidase. The reaction conditions are listed in Table 2. After 2, 4, 8, 16, 18, 24, 25, 26, 27 and 28 h, the amounts of α-L-Fuc-D-Man produced in the reaction mixtures were measured by HPLC with a Hiber LiChroCART NH_2 column (Fig. 1). As shown in Figure 2, the maximum yield of α-L-Fuc-D-Man was obtained with an enzyme concentration of 0.300 U/mL α-fucosidase (**B**) after 27 h.

2.1.4. Characterisation

High-resolution mass spectroscopy of **1** (*m/z* 327.1291; M+H) indicated a molecular formula consistent with α-L-Fuc-D-Man. NMR analysis was performed using ^{1}H–^{1}H COSY, ^{1}H–^{13}C COSY and homo decoupling, and nuclear Overhauser effect (NOE) difference spectra; all carbons in the spectrum of **1** were completely assigned. Figure 3 shows the ^{1}H–^{13}C COSY spectrum of **1** in D_2O. The signals due to the α-L-fucosylated C-3 of D-Man (M-3α, M-3β) shifted downfield by 7–8 ppm compared with the signal of D-Man. The H-1 signal of α-L-Fuc was observed at δ 4.58, with a $J_{1,2}$ value of 8.20 Hz; furthermore, the NOESY spectrum indicated that α-L-Fuc was bound through an α-(1→3)-linkage to D-Man.

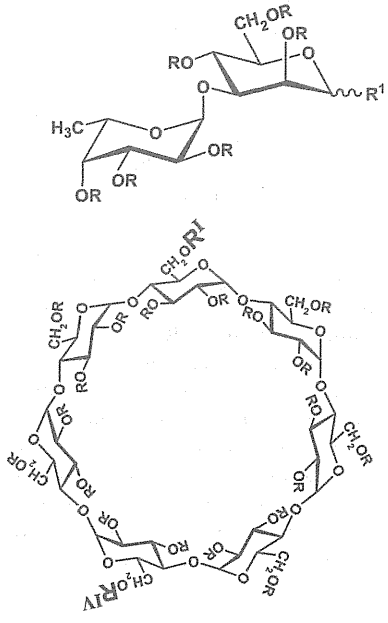

1 R = H, R^1 = OH
2 R = Ac, R^1 = OAc (α)
3 R = Ac, R^1 = OC(NH)CCl_3

	R^{I}	R^{IV}	R
4	Si	Si	Ac
5	H	H	Ac
6	α-Fuc-Man	α-Fuc-Man	H
7	α-Fuc-Man	H	H
8	α-Fuc-α-Man	α-Fuc-α-Man	H
9	α-Fuc-α-Man	H	H
10	α-Fuc	α-Fuc	H
11	α-Fuc	H	H

Si : *tert*-butyldimethylsilyl
α-Fuc-Man : α-L-Fuc-(1→3)-D-Man
α-Fuc-α-Man : α-L-Fuc-(1→3)-α-D-Man

Chart 1.

Table 1
Partial purification of α-fucosidase

	Fraction	Protein		α-Fucosidase			
	Volume (mL)	Concentration (mg/mL)	Total amount (mg)	Activity (U/mL)	Total activity (U)	Specific activity (U/mg)	Recovery factor (%)
I	126	22	2772	3.39	427	0.154	100
II	610	3.39	2065	0.658	401	0.194	93.9
III	29	23.3	675	11.8	342	0.506	80.1

Table 2
Reaction conditions of α-fucosidase on *p*-nitrophenyl α-L-fucopyranoside and D-mannose

α-Fucosidase activity		1.0% (18.4 mM) *p*-NP α-l-Fuc	10% (87.8 mM) d-Mannose	0.2 M Sodium acetate buffer (pH 4.0)
U/mL	μL	μL (μmol)	μL (μmol)	μL
0.118	300	1000 (35.1)	300 (166)	300
0.3	150	500 (17.5)	150 (83.3)	150
0.5	150	500 (17.5)	150 (83.3)	150

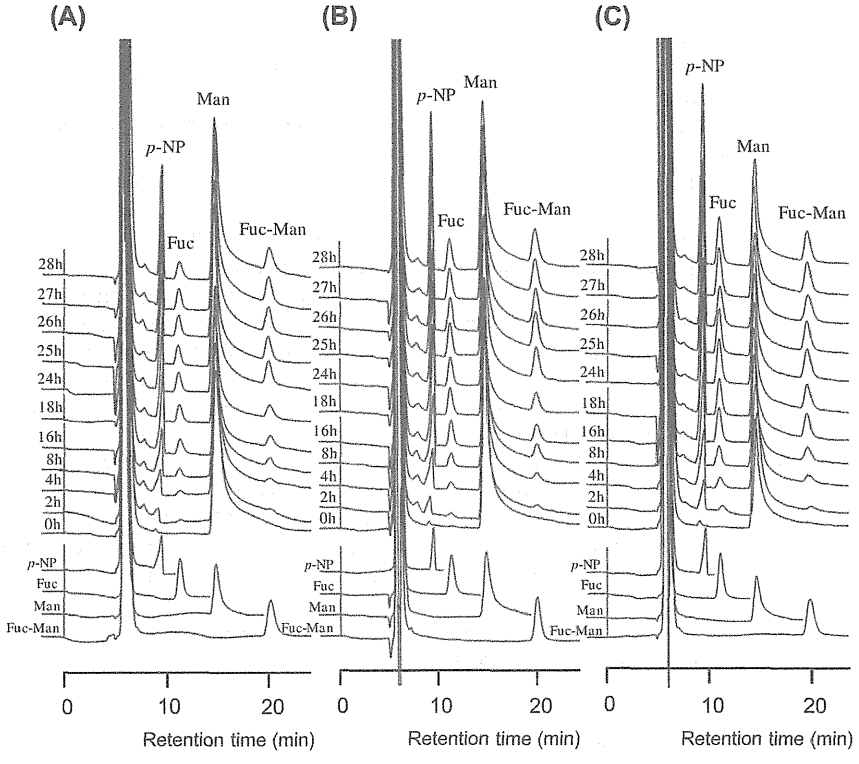

Figure 1. The elution profiles of α-L-fucopyranosyl-D-mannopyranose (Fuc-Man), L-fucose (Fuc), D-mannose (Man) and *p*-nitrophenol (*p*-NP). Chromatographic conditions: column, LiChroCART NH_2 (250 × 4.0 mm i.d.); eluent, acetonitrile/water (77:23, v/v); flow rate, 0.5 mL/min; detector, shodex RI-101; temperature, 30 °C. (A) α-fucosidase (0.118 U/mL); (B) α-fucosidase (0.300 U/mL); (C) α-fucosidase (0.500 U/mL).

Based on these results, compound **1** was identified as 3-*O*-α-L-fucopyranosyl-D-mannopyranose [α-L-Fuc-(1→3)-D-Man] with a **1α**:**1β** ratio of 2.5:1.

2.2. Preparation, separation and characterisation of $6^{I},6^{IV}$-di-*O*-(3-*O*-α-L-fucopyranosyl-α-D-mannopyranosyl)-cyclomaltoheptaose {8, $6^{I},6^{IV}$-di-*O*-[α-L-Fuc-(1→3)-α-D-Man]-βCD} and 6-*O*-(3-*O*-α-L-fucopyranosyl-α-D-mannopyranosyl)α-cyclomaltoheptaose {9, 6-*O*-[α-L-Fuc-(1→3)-α-D-Man]-βCD}

The glycosyl acceptor, bis(2,3-di-*O*-acetyl)-pentakis(2,3,6-tri-*O*-acetyl)-βCD (**5**), was obtained from $6^{I},6^{IV}$-di-*O*-(*t*-$BuMe_2Si$)-βCD peracetate (**4**),[27] whose structure was previously established. Acetylation of **1** with acetic anhydride-pyridine and then selective 1-*O*-deacetylation[28] of the fully acetylated disaccharide (**2**) with hydrazine acetate in dry *N*,*N*-dimethylformamide afforded 2,3,4-tri-*O*-acetyl-α-L-fucopyranosyl-(1→3)-2,4,6-tri-*O*-acetyl-D-mannopyranose (**2′**). 2,3,4-Tri-*O*-acetyl-α-L-fucopyranosyl-(1→3)-2,4,6-tri-*O*-acetyl-D-mannopyranosyl trichloroacetimidate (**3**) was obtained by treatment of **2′** with trichloroacetonitrile in the presence of 1,8-diazabicyclo[5.4.0]-undec-7-ene (DBU) in dichloromethane. Glycosylation of **5** with **3** in dichloromethane in the presence of trimethylsilyl trifluoromethanesulfonate (TMSOTf) as an acid catalyst gave a di-branched βCD derivative containing two disaccharides and a mono-branched βCD derivative with one disaccharide. These compounds were fractionated by centrifugal chromatography, followed by deacetylation with methanolic sodium methoxide and isolation by HPLC on a TSKgel Amide-80 column and a DAISOPAK

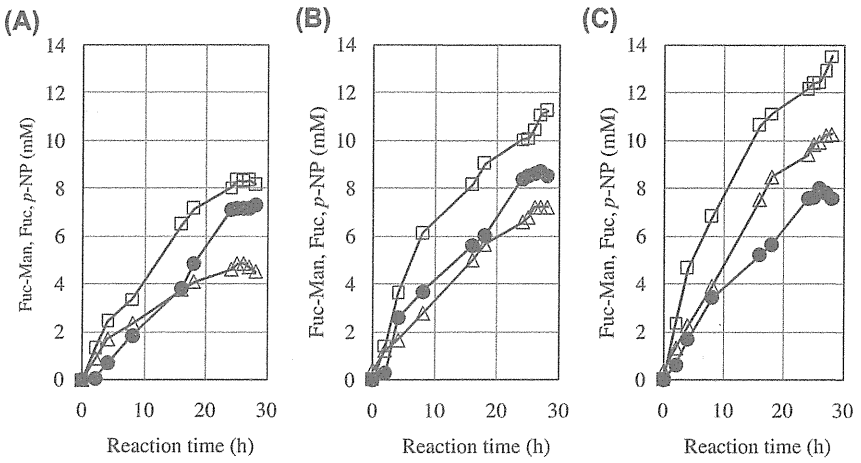

Figure 2. Effects of enzyme concentration on the formation of α-L-fucopyranosyl-D-mannopyranose (Fuc-Man). Reaction mixtures were analysed by HPLC. Reaction mixtures containing 10% D-Man and 1.0% 4-nitrophenyl α-L-fucopyranoside in 0.2 M sodium acetate buffer (pH 4.0) were incubated with α-fucosidase at varying concentrations: 0.118 U/mL (A), 0.300 U/mL (B), 0.500 U/mL (C), at 40 °C. (●), Fuc-Man; (□), *p*-nitrophenol (*p*-NP); (△), L-fucose (Fuc).

SP-ODS-BP column to produce $6^{I},6^{IV}$-di-*O*-[α-L-Fuc-(1→3)-D-Man]-βCD (**6**) and 6-*O*-[α-L-Fuc-(1→3)-D-Man]-βCD (**7**). MALDI-TOF-MS analysis of **6** (*m/z* 1773.65; M+Na) and **7** (*m/z* 1465.51; M+Na) confirmed the molecular formulas of di-branched βCD and mono-branched βCD, respectively. NMR analysis was performed using ^{1}H–^{1}H COSY, ^{1}H–^{13}C COSY, homo decoupling and NOE difference spectra, and all carbons in the spectra of **6** and **7** were completely assigned (Fig. 4). The assignments of the C-6 signals were detected by the DEPT (distortionless enhancement by polarisation transfer) method.[29] In the spectra of **6** and **7**, the signals due to the glycosylated C-6 (G′-6, δ 67.46 and 67.52) were shifted downfield by 6–7 ppm compared with the C-6 signals (G-6, δ 61.00–61.14) of the five or six unsubstituted βCD ring glucoses. The C-1 signals (M-1, δ 100.93–100.96) of D-Man ($^{1}C_4$ chair conformation) were shifted upfield compared to the C-1 signals of the βCD ring (G-1 and G′-1, δ 102.59–102.69). In the case of D-Man[6,30] residues ($^{4}C_1$ chair conformation) bonded to the CD ring via α-(1→6)-linkage, the C-1 signals of D-Man were shifted upfield compared to the C-1 signals of the CD ring. In addition, the H-1 signals of D-Man were observed at δ 4.92 (br s); furthermore, the NOESY spectra indicated that α-L-Fuc-(1→3)-D-Man was bound through an α-linkage to the CD ring. Based on these results, compounds **6** and **7** were identified as {$6^{I},6^{IV}$-di-*O*-[α-L-Fuc-(1→3)-α-D-Man]-βCD} (**8**) and {6-*O*-[α-L-Fuc-(1→3)-α-D-Man]-βCD} (**9**), respectively.

2.3. Biological effects of the fucosyl βCD derivatives on a colon cancer cell line, HCT116

2.3.1. The effects of the fucosyl βCD derivatives on cell viability

To evaluate the availability of the fucosyl βCD derivatives as potential carriers for a drug delivery system, their cell toxicity was examined in a colon cancer cell line, HCT116. After culturing for 72 h with $6^{I},6^{IV}$-di-*O*-(α-L-Fuc)-βCD (**10**), 6-*O*-(α-L-Fuc)-βCD (**11**) and βCD, the viable cell number was quantified using a WST assay. As shown in Figure 5A, cell growth was slightly yet significantly increased in the presence of **10** but not with **11** or βCD compared to the control cells with no treatment. When the cells were cultured in the presence of **8** and **9**, which were synthesised in this study, a similar increase of cell growth was observed in the presence **8** but not with **9** (Fig. 5B). Interestingly, both derivatives (**8** and **10**) that have two branched α-L-Fuc-α-D-Man or α-L-Fuc residues showed a stimulatory effect on cell growth. In Figure 6, the concentration-dependent cell toxicity for **10** and βCD is compared. As shown in Figure 5A, the stimulatory effect on cell growth by **10** was observed at the concentration below 4 mM. Although high concentrations of **10** caused some cell toxicity, interestingly, the toxicity was significantly less than that by βCD.

2.3.2. Effects of the fucosyl βCD derivatives on cellular fucosylation

Cellular fucosylation has been reported to be involved in cell growth.[31] In this study, we examined whether the fucosyl βCD derivatives affect cellular fucosylation. HCT116 cells show a deficiency of fucosylation because of a deletion mutation in the GMDS gene, which is an essential enzyme for GDP-fucose synthesis via the de novo pathway. The addition of exogenous L-Fuc into the culture media of HCT116 cells dramatically restored cellular fucosylation (Fig. 7) indicating that the salvage pathway, another pathway for GDP-fucose synthesis, is intact in the cells. When the cells were cultured in the presence of **8**, **9**, **10** and **11**, increased fucosylation was observed in the fucosyl βCD derivatives with two branches of α-L-Fuc-α-D-Man or α-L-Fuc (**8** and **10**) compared to those with only one branch (**9** and **11**). No difference was observed for the restoration of cellular fucosylation with **8** and **10**. The strong restoration of cellular fucosylation by the fucosyl βCD derivatives with two branches of α-L-Fuc-α-D-Man or α-L-Fuc (**8**, **10**) might be related to the previously observed increase in cell growth and decrease in toxicity. However, the restoration of fucosylation by wild type GMDS[22] and free L-Fuc (Fig. 8) did not cause any change in cell growth, suggesting that fucosylation as well as some other constituent of the compounds are required for the growth-promoting effects and decreased toxicity observed for the fucosyl βCD derivatives. The mechanism underlying growth-promoting effect and low toxicity of two branched fucosyl βCDs should be investigated in more detail in a future study.

Two types of fucosidase have been reported in humans: α-L-fucosidase 1 (FUCA1) and 2 (FUCA2). FUCA1 and 2 are localised in lysosomes and secreted into extracellular spaces, respectively, where they catalyse the hydrolysis of α-L-Fuc residues linked to other monosaccharides. As shown in Figure 9, the expression of FUCA1 and 2 in HCT116 cells was confirmed by RT-PCR analysis in the absence and presence of the fucosyl βCD derivatives. There are two possible mechanisms by which the fucosyl βCD derivatives with two branches of α-L-Fuc-α-D-Man or α-L-Fuc (**8**, **10**) efficiently restore fucosylation. First, the branched α-L-Fuc residues are efficiently detached by FUCA2 and then transported into the cytosol where they are used for GDP-fucose synthesis. Alternatively, the fucosyl βCD derivatives are internalised and transported into lysosomes by an endocytosis pathway, and the free α-L-Fuc residues produced by the hydrolytic reaction with FUCA1 are reused for

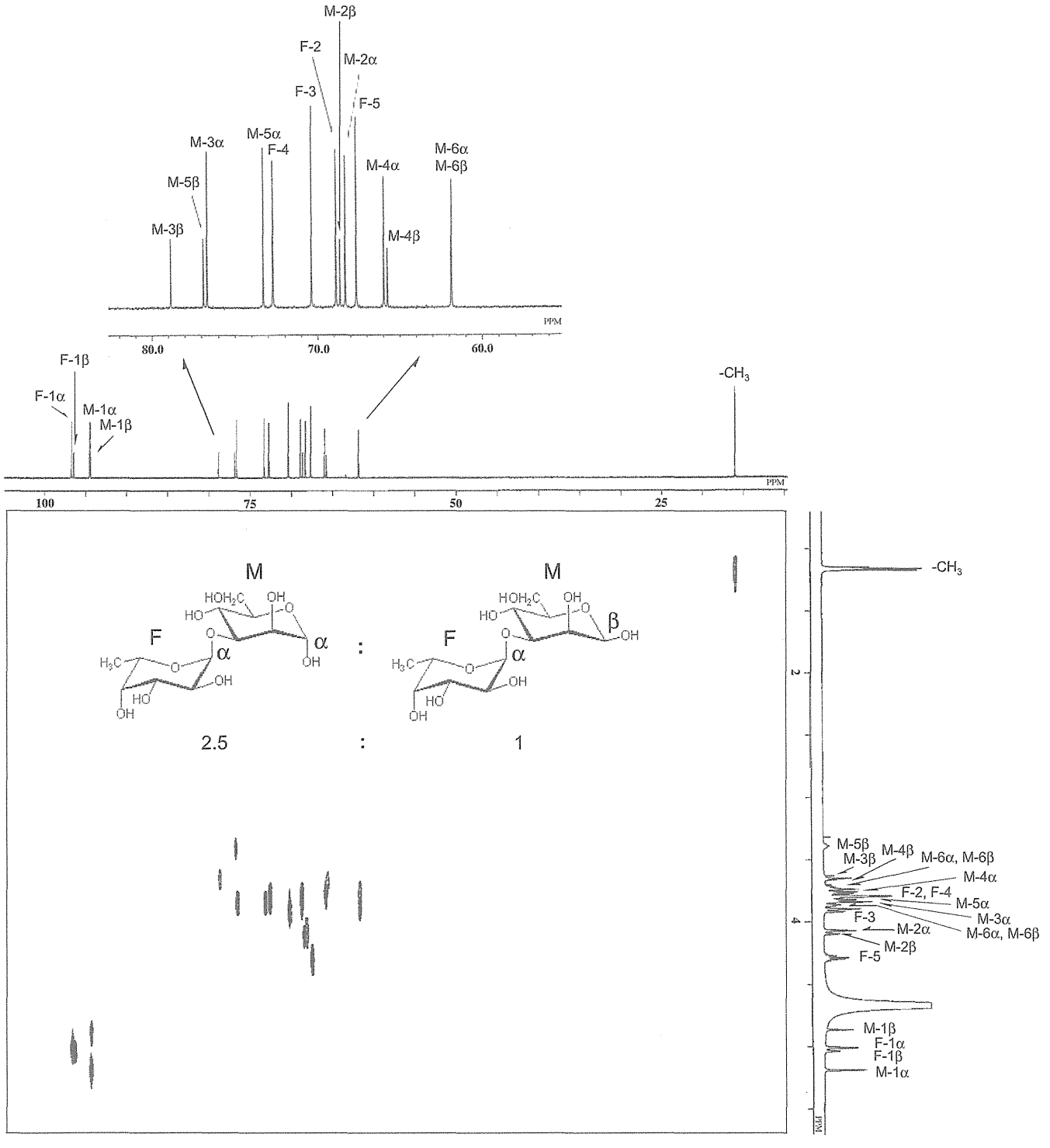

Figure 3. ^{1}H–^{13}C COSY, spectra of α-L-fucopyranosyl-(1→3)-D-mannopyranose (1α and 1β) measured in D_2O at 125 MHz.

GDP-fucose synthesis in the cytosol. In fact, reports suggest that the βCD derivatives can be transported to the lysosomes.[32] Further studies are needed to identify the correct mechanism.

3. Experimental

3.1. General methods

HPLC was performed using a PU-980, PU-880 pump (Jasco) or a LC-10AD pump (Shimadzu), a Rheodyne 7125 injector, and a Shodex RI-71 or RI-101 refractive index monitor (Showa Denko), or a RID-10A refractive index monitor (Shimadzu). HPLC analysis was conducted at constant temperature using a CA-202 (Flom) or CTO-20AC (Shimadzu) column oven. The columns employed were a YMC-Pack SH-343-7 ODS (250 × 20 mm i.d.), a YMC A-312 ODS (150 × 6.0 mm i.d.), a DAISOPAK SP-120-5-ODS-BP (150 × 4.6 mm i.d.), a DAISOPAK SP-120-5-ODS-BP (250 × 10 mm i.d., 250 × 20 mm i.d.), a DAISOPAK SP-100-5-ODS-P (150 × 4.6 mm i.d.), a Hibar LiChroCART NH_2 (250 × 4.0 mm i.d., Kanto Chemical), a TSKgel Amide-80 (300 × 7.8 mm i.d., Tosoh) and a COSMOSIL

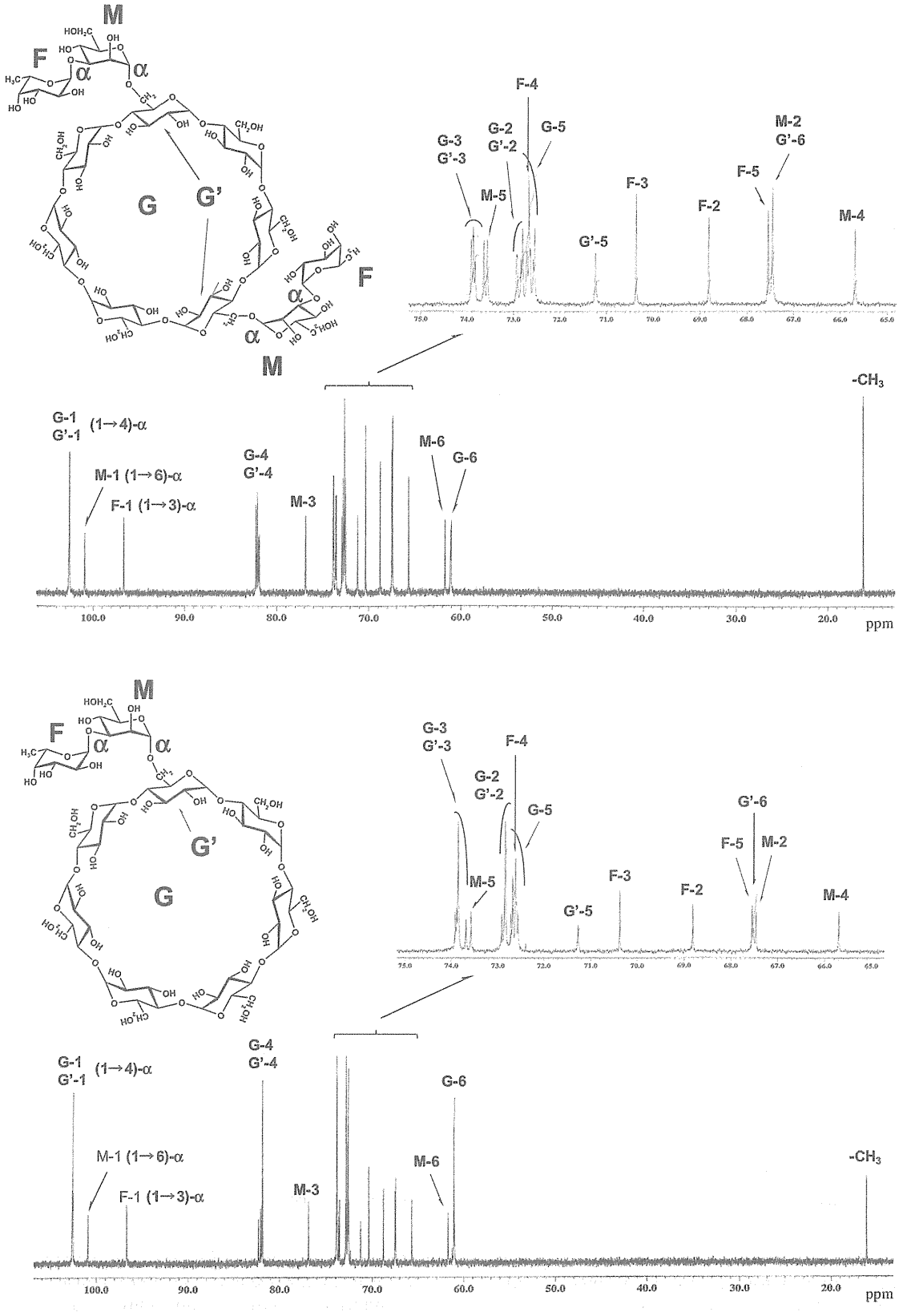

Figure 4. ^{13}C NMR spectra of $6^{I},6^{IV}$-di-*O*-[α-L-Fuc-(1→3)-α-D-Man]-βCD (**8**) and 6-*O*-[α-L-Fuc-(1→3)-α-D-Man]-βCD (**9**) measured in D_2O at 125 MHz.

$5C_{18}$-MS-II (150 × 4.6 mm i.d.). ^1H and ^{13}C NMR spectroscopic data were recorded in D_2O or $CDCl_3$ using a Jeol GSX-500 or Jeol JNM-ECP 500 spectrometer (^1H: 500 MHz, ^{13}C: 125 MHz). The chemical shifts are expressed in ppm downfield from a Me_4Si signal and referenced to an external 1,4-dioxane (67.4 ppm) signal. The conditions for the ^1H–^1H COSY and ^1H–^{13}C COSY measurements were the same as those described in a previous paper.[33] HRFAB-MS was measured in positive-ion mode using a Jeol MS 700 mass

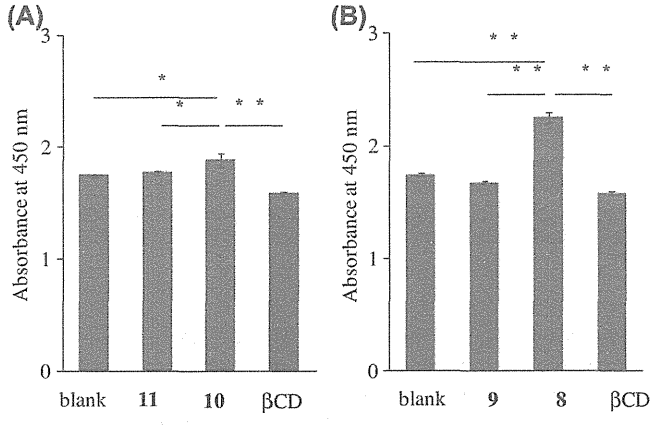

Figure 5. The growth rate of HCT116 cells treated with 1 mM of fucosyl βCDs. At 72 h after the addition of 6^{I},6^{IV}-di-*O*-[α-L-Fuc-(1→3)-α-D-Man]-βCD (**8**), 6-*O*-[α-L-Fuc-(1→3)-α-D-Man]-βCD (**9**), 6^{I},6^{IV}-di-*O*-(α-L-Fuc)-βCD (**10**) and 6-*O*-(α-L-Fuc)-βCD (**11**), the growth rate of the HCT116 cells was investigated using a WST assay. Error bars represent ± SD.*p <0.05, **p <0.01.

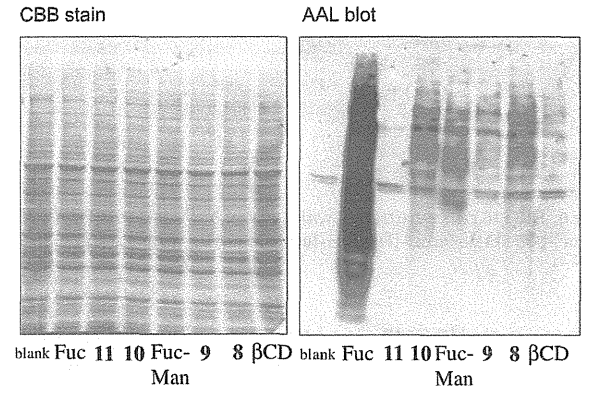

Figure 7. HCT116 cells were treated with 1 mM of 6^{I},6^{IV}-di-*O*-[α-L-Fuc-(1→3)-α-D-Man]-βCD (8), 6-*O*-[α-L-Fuc-(1→3)-α-D-Man]-βCD (**9**), 6^{I},6^{IV}-di-*O*-(α-L-Fuc)-βCD (**10**), 6-*O*-(α-L-Fuc)-βCD (**11**), L-fucose (Fuc), α-L-fucopyranosyl-D-mannopyranose (Fuc-Man) and βCD, and the expression patterns of the fucosylated glycoproteins in the cells were investigated by AAL blot analysis. Coomassie brilliant blue (CBB) staining indicated that equal amounts of protein were loaded into each lane.

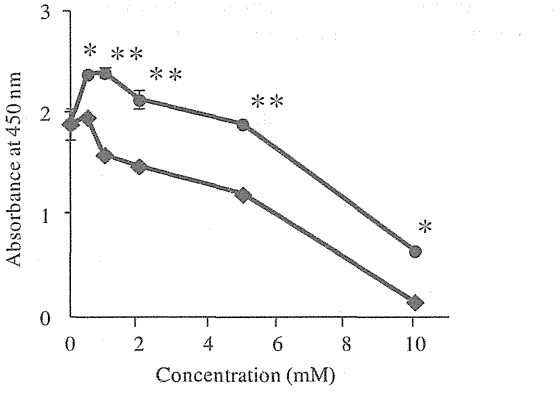

Figure 6. The dose-dependent effect of fucosyl βCD and βCD on the growth of HCT116 cells. After 72 h of treatment with 6^{I},6^{IV}-di-*O*-(α-L-Fuc)-βCD (**10**) and βCD, the growth rate was investigated using a WST assay. (●), 6^{I},6^{IV}-di-*O*-(α-L-Fuc)-βCD (**10**); (♦), βCD. Error bars represent ± SD. *p <0.05, **p <0.01.

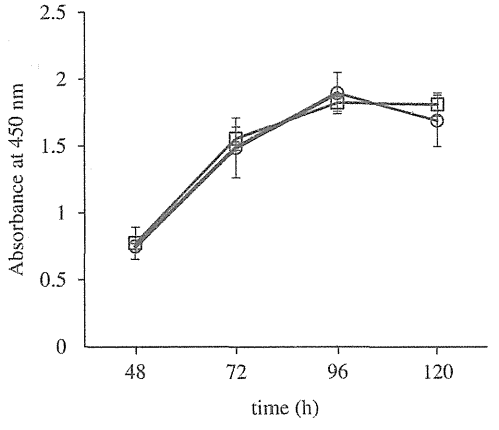

Figure 8. The effect of free L-fucose on in vitro cell growth. Cells were plated at 2500 cells/well in 96 well plates and cultured for the indicated time in the absence (○) or presence (□) of free L-fucose. Cell growth was determined by a WST assay. Error bars represent ± SD.

spectrometer with xenon atoms and a glycerol matrix. MALDI-TOF-MS was performed on a Vision 2000 instrument (Thermo Bioanalysis) using 2,5-dihydroxybenzoic acid as the matrix. The instrument was operated in positive-ion reflection mode with an accelerating potential of 7 kV. Optical rotations were determined with a Jasco P-1020 polarimeter at 26 °C. TLC was performed on Silica Gel 60 plates (E. Merck). The melting points were measured using a Yanagimoto micro melting-point apparatus and were uncorrected. A UVIDEC V-530 double beam spectrophotometer (Jasco) was used to determine absorbance. Centrifugal chromatography was performed with a Harrison Centrifugal Thin-Layer Chromatotron 7924.

3.2. Syntheses of substrates

3.2.1. α-L-Fucopyranosyl-(1→3)-D-mannopyranose (1)

A mixture of 4-nitrophenyl α-L-fucopyranoside (500 mg, 1.75 mmol) and D-Man (1.5 g, 8.33 mmol) was suspended in 15 mL of 0.2 M sodium acetate buffer (pH 4.0) and incubated with 15 mL of α-fucosidase (0.300 unit/mL), which was purified partially from Sumizyme PHY (Shin Nihon Chemical Co., Ltd) at 40 °C for 27 h. The reaction mixture was heated at 100 °C for 20 min to stop enzyme action. This reaction was repeated three times. Then, the reaction mixture was placed on an active carbon column (33 × 3.4 cm i.d.). After the column was washed with H_2O to remove D-Man and L-Fuc, compound **1** was eluted using a linear gradient from zero to 7% aqueous ethanol solution (1.5 L of each). Further isolation of compound **1** was achieved with preparative HPLC using a column of TSKgel Amide-80 with 73:27 MeCN/water. The yield was 364 mg (23.4%). Analysis of **1** by HPLC on a Hi-bar LichroCART NH_2 with 77:23 MeCN/water showed a single peak. Compound **1α**: ^{1}H NMR (500 MHz, D_2O) δ: 5.19 (1H, br d, $J_{1,2}$ = 1.9 Hz, M-1), 5.01 (1H, d, $J_{1,2}$ = 3.7 Hz, F-1), 4.29 (1H, q, J = 6.6 Hz, F-5), 4.07 (1H, br t, J = 2.8, 2.5 Hz, M-2), 3.91 (1H, dd, J = 10.5, 2.8 Hz, F-3), 3.88 (1H, dd, J = 12.3, 2.2 Hz, M-6), 3.83 (1H, dd, J = 9.6, 2.8 Hz, M-3), 3.82 (1H, m, M-5), 3.78 (1H, dd, J = 10.5, 3.7 Hz, F-2), 3.75 (1H, br d, J = 2.8 Hz, F-4), 3.74 (1H, t, J = 9.6 Hz, M-4), 3.72 (1H, dd, J = 12.4, 6.3 Hz, M-6), 1.17 (3H, d, J = 6.6 Hz, F-6); ^{13}C NMR (125 MHz, D_2O) δ: 96.72 (F-1), 94.52 (M-1), 76.67 (M-3), 73.29 (M-5), 72.73 (F-4), 70.37 (F-3), 68.87 (F-2), 68.30 (M-2), 67.64 (F-5), 65.97 (M-4), 61.83 (M-6), 16.07 (F-6); Compound **1β**: ^{1}H NMR (500 MHz, D_2O) δ: 5.03 (1H, d, $J_{1,2}$ = 4.1 Hz, F-1), 4.86 (1H, br d, $J_{1,2}$ = 0.9 Hz, M-1), 4.29 (1H, q, J = 6.6 Hz, F-5), 4.09 (1H, dd like, M-2), 3.91 (1H, dd, J = 10.5, 2.8 Hz, F-3), 3.88 (1H, dd, J = 12.3, 2.2 Hz, M-6), 3.78 (1H, dd, J = 10.5, 3.7 Hz, F-2), 3.75 (1H, br d, J = 2.8 Hz, F-4), 3.72 (1H, dd, J = 12.4, 6.3 Hz, M-6), 3.66–3.63 (2H, m, M-3, M-4), 3.39 (1H, m, M-5), 1.16 (3H, d,

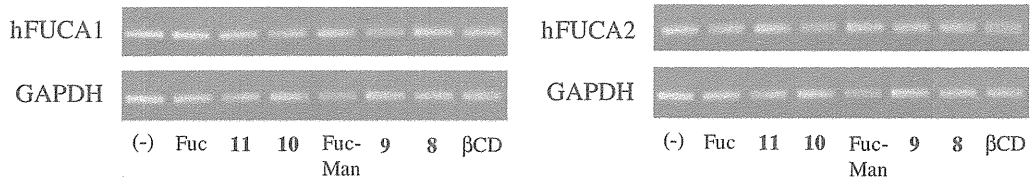

Figure 9. HCT116 cells were treated with 1 mM of 6^{I},6^{IV}-di-*O*-[α-L-Fuc-(1→3)-α-D-Man]-βCD (**8**), 6-*O*-[α-L-Fuc-(1→3)-α-D-Man]-βCD (**9**), 6^{I},6^{IV}-di-*O*-(α-L-Fuc)-βCD (**10**), 6-*O*-(α-L-Fuc)-βCD (**11**), L-fucose (Fuc), α-L-fucopyranosyl-D-mannopyranose (Fuc-Man) and βCD, and the expression of hFUCA1 and hFUCA2 in the cells was investigated by RT-PCR.

J = 6.3 Hz, F-6); ^{13}C NMR (125 MHz, D_2O) δ: 96.43 (F-1), 94.43 (M-1), 78.85 (M-3), 76.89 (M-5), 72.71 (F-4), 70.37 (F-3), 68.86 (F-2), 68.62 (M-2), 67.64 (F-5), 65.74 (M-4), 61.83 (M-6), 16.07 (F-6); HRFAB-MS Calcd for $C_{12}H_{23}O_{10}$ (M+H): 327.1291. Found: 327.1291.

3.2.2. 2,3,4-Tri-*O*-acetyl-α-L-fucopyranosyl-(1→3)-1,2,4,6-tetra-*O*-acetyl-α-D-mannopyranose (2)

Acetylation of compound **1** (571 mg, 1.75 mmol) was performed with a mixture of Ac_2O (13 mL) and dry pyridine (25 mL), which were stirred overnight at rt. The mixture was concentrated, and the residue was extracted with $CHCl_3$. The extract was washed sequentially with ice-cold aqueous $NaHCO_3$ and water. The extract was dried ($CaCl_2$) and concentrated to produce a syrup (934 mg). Crystallisation of the syrup from EtOH gave **2** as colourless crystals (828 mg, 76.2%). Compound **2**: R_f 0.67 (1:1 hexane/acetone); mp 221.6–222.3 °C; $[\alpha]_D^{26}$, −64.87° (*c* 1.0, $CHCl_3$); ^{1}H NMR (500 MHz, $CDCl_3$) δ: 6.08 (1H, d, $J_{1,2}$ = 2.3 Hz, M-1), 5.35 (1H, t, *J* = 9.8 Hz, M-4), 5.28 (1H, dd, *J* = 3.0, 1.5 Hz, F-4), 5.21 (1H, dd, *J* = 10.0, 2.8 Hz, F-3), 5.19 (1H, dd, *J* = 8.7, 3.2 Hz, F-2), 5.18 (1H, br t, *J* = 2.8 Hz, M-2), 5.15 (1H, d, $J_{1,2}$ = 3.3 Hz, F-1), 4.24 (1H, dd, *J* = 12.5, 5.4 Hz, M-6), 4.18 (1H, qd, *J* = 6.4, 4.1 Hz, F-5), 4.12 (1H, dd, *J* = 12.5, 2.7 Hz, M-6), 4.09 (1H, dd, *J* = 10.0, 2.9 Hz, M-3), 3.96 (1H, m, *J* = 9.8, 5.2, 2.7 Hz, M-5), 2.17, 2.16, 2.14, 2.12, 2.09, 2.06, 1.96 (3H, s, –$COCH_3$), 1.15 (3H, d, *J* = 6.6 Hz, F-6); ^{13}C NMR (125 MHz, $CDCl_3$) δ: 170.63, 170.47, 170.36, 169.87, 169.60, 169.38, 167.97 (7C, –$OCOCH_3$), 95.75 (F-1), 90.70 (M-1), 73.07 (M-3), 71.03 (F-4), 70.95 (M-5), 67.68 (M-2, F-3), 67.51 (F-2), 67.04 (M-4), 65.43 (F-5), 62.38 (M-6), 20.83, 20.83, 20.72, 20.70, 20.70, 20.60, 20.58 (7C, –$COCH_3$), 16.07 (F-6). HRFAB-MS Calcd for $C_{26}H_{37}O_{17}$ (M+H): 621.2031. Found: 621.2029. Anal. Calcd for $C_{26}H_{36}O_{17}$: C, 50.27; H, 5.94. Found: C, 50.32; H, 5.85.

3.2.3. 2,3,4-Tri-*O*-acetyl-α-L-fucopyranosyl-(1→3)-2,4,6-tri-*O*-acetyl-D-mannopyranosyl trichloroacetimidate (3)

Compound **2** (610 mg, 0.98 mmol) was stirred with hydrazine acetate (135 mg, 1.47 mmol) in dry DMF (15 mL) for 2 h at 0–16 °C. The mixture was then diluted with EtOAc and washed with aqueous NaCl and ice-water, and the organic layer was dried with $MgSO_4$ and concentrated to give 2,3,4-tri-*O*-acetyl-α-L-fucopyranosyl-(1→3)-2,4,6-tri-*O*-acetyl-D-mannopyranose (**2′**) as a syrup (569 mg, 100%); R_f 0.55 (1:1 hexane/acetone). To a mixture of **2′** (569 mg, 0.98 mmol) with dry 4 Å molecular sieves (1.5 g) in dry CH_2Cl_2 (10 mL) was added DBU (30 μL, 0.20 mmol) and trichloroacetonitrile (990 μL, 9.9 mmol), and the mixture was stirred for 1 h at 0 °C. The reaction mixture was diluted with $CHCl_3$, washed with ice water, dried ($CaCl_2$) and concentrated. Centrifugal chromatography of the residue (3:1 → 1:1, hexane/acetone) yielded **3** (573 mg, 80.6%). R_f 0.58 (1:1 hexane/acetone).

3.2.4. Bis(2,3-di-*O*-acetyl)-pentakis(2,3,6-tri-*O*-acetyl)-cyclomaltoheptaoses (5)

Ac_2O (10 mL) was added to a solution of 6^{I},6^{IV}-di-*O*-(*t*-$BuMe_2Si$)-βCD (582 mg, 0.43 mmol) in dry pyridine (30 mL), and the mixture was stirred for 5 h at 100 °C and then concentrated. The residue was extracted with $CHCl_3$, and the extract was washed sequentially with aqueous $NaHCO_3$ and water, dried with $CaCl_2$ and concentrated to 6^{I},6^{IV}-di-*O*-(*t*-$BuMe_2Si$)-βCD peracetate (**4**). In an ice-water bath, $BF_3{\cdot}Et_2O$ (635 μL) was added to a solution of **4** in dry $CHCl_3$ (37 mL) while stirring, and stirring was continued for 4 h at rt. The $CHCl_3$ solution was washed with water, aqueous $NaHCO_3$ and water again, dried ($CaCl_2$) and concentrated to produce **5** (663 mg, 80.3%). R_f 0.44 (2:3 hexane/acetone).

3.2.5. 6^{I},6^{IV}-Di-*O*-[α-L-fucopyranosyl-(1→3)-α-D-mannopyranosyl]-cyclomaltoheptaose (8) 6-*O*-[α-L-fucopyranosyl-(1→3)-α-D-mannopyranosyl]-cyclomaltoheptaose (9)

A mixture of **5** (500 mg, 0.26 mmol) and **3** (573 mg, 0.79 mmol) with dry powder 4 Å molecular sieves (type AW300, 2 g) in dry CH_2Cl_2 (33 mL) was stirred under argon at −20 °C, and a solution of TMSOTf (100 μL) in dry CH_2Cl_2 (2 mL) was added. After stirring for 2 h at −20 °C, triethylamine (1 mL) was added to the mixture, which was then diluted with $CHCl_3$, filtered through Celite, washed sequentially with 1 M H_2SO_4, aqueous $NaHCO_3$ and water, dried and concentrated. The residue was fractionated by centrifugal chromatography with 3:1 → 2:1 → 3:2 → 1:1 hexane/acetone to yield fractions containing 6^{I},6^{IV}-di-*O*-[2,3,4-tri-*O*-acetyl-α-L-fucopyranosyl-(1→3)-2,4,6-tri-*O*-acetyl-D-mannopyranosyl]-βCD peracetate and the mono-glycosylated βCD derivative **A** (524 mg). Each fraction was individually treated with 0.5 M methanolic CH_3ONa (1.0–3.0 mL) for 2 h at rt, neutralised with Amberlite IR-120B (H^+) resin, filtered and concentrated to produce 6^{I},6^{IV}-di-*O*-[α-L-Fuc-(1→3)-D-Man]-βCD (**6**) and 6-*O*-[α-L-Fuc-(1→3)-D-Man]-βCD (**7**). Each mixture was purified by HPLC on a TSKgel Amide-80 column with 3:2 MeCN/water to yield 6^{I},6^{IV}-di-*O*-[α-L-Fuc-(1→3)-α-D-Man]-βCD (**8**, 160 mg) and 6-*O*-[α-L-Fuc-(1→3)-α-D-Man]-βCD (**9**, 60 mg). Analysis of **8** and **9** by HPLC using a COSMOSIL 5C^{18}-MS-II column with 5:95 MeOH/water showed a single peak for each fraction. Compound **8**: $[\alpha]_D^{26}$, +68.71° (*c* 1.0, H_2O); ^{1}H NMR (500 MHz, D_2O) δ: 5.05 (5H, d, $J_{1,2}$ = 3.7 Hz, G-1), 5.03 (4H, d, $J_{1,2}$ = 3.7 Hz, F-1, G′-1), 4.92 (2H, br s, M-1), 4.31 (2H, q, *J* = 6.6 Hz, F-5), 4.15 (2H, br t, *J* = 2.2 Hz, M-2), 4.02–4.06 (2H, m, G′-6), 3.97 (2H, m, G′-5), 3.93 (7H, br t, *J* = 9.2 Hz, G-3, G′-3), 3.92 (2H, dd, *J* = 10.6, 3.7 Hz, F-3), 3.91–3.93 (5H, m, G-6), 3.86–3.89 (2H, m, M-6), 3.84–3.86 (5H, m, G-6), 3.83 (2H, dd, *J* = 9.2, 3.2 Hz, M-3), 3.82 (5H, m, G-5), 3.82 (2H, d, *J* = 3.2 Hz, F-5), 3.82–3.84 (2H, m, G′-6), 3.81 (2H, dd, *J* = 10.6, 3.2 Hz, F-2), 3.79 (2H, t, *J* = 9.2 Hz, M-4), 3.75–3.80 (2H, m, M-6), 3.73–3.75 (2H, m, M-5), 3.63 (7H, dd, *J* = 9.5, 3.7 Hz, G-2, G′-2), 3.57 (7H, br t, *J* = 8.7 Hz, G-4, G′-4), 1.19 (6H, d, *J* = 6.6 Hz, F-6); ^{13}C NMR (125 MHz, D_2O) δ: 102.69–102.63 (7C, G-1, G′-1), 100.96, 100.94 (2C, M-1), 96.68, 96.66 (2C, F-1), 82.25–81.88 (7C, G-4, G′-4), 76.90, 76.88 (2C, M-3), 73.91–73.64 (7C, G-3, G′-3), 73.57 (2C, M-5), 72.94–72.54 (13C, G-2, G′-2, G-5), 72.71–72.64 (2C, F-4), 71.23 (1C, G′-5), 70.37 (2C, F-3), 68.81 (2C, F-2), 67.55 (2C, F-5), 67.46 (3C, M-2, G′-6), 65.69 (2C, M-4), 61.72 (2C, M-6), 61.14–61.03 (6C, G-6), 16.11 (2C, F-6); HRFAB-MS Calcd for $C_{66}H_{109}O_{53}$ (M-H): 1749.5384. Found: 1749.5842; Compound **9**: $[\alpha]_D^{26}$, +87.97° (*c* 1.0, H_2O); ^{1}H NMR (500 MHz, D_2O), δ: 5.06 (6H, d, $J_{1,2}$ = 3.7 Hz, G-1),

5.04 (1H, d, J = 3.7 Hz, G′-1), 5.03 (1H, d, $J_{1,2}$ = 3.7 Hz, F-1), 4.92 (1H, br s, M-1), 4.32 (1H, q, J = 6.8 Hz, F-5), 4.14 (1H, dd like, M-2), 4.02–4.05 (1H, m, G′-6), 3.97–3.99 (1H, m, G′-5), 3.93 (7H, t, J = 9.7 Hz, G-3, G′-3), 3.92 (1H, dd, J = 10.1, 3.2 Hz, F-3), 3.91–3.93 (6H, m, G-6), 3.86–3.88 (6H, m, G-6), 3.83–3.86 (1H, m, G′-6), 3.83 (1H, dd, J = 9.2, 3.3 Hz, M-3), 3.82–3.84 (6H, m, G-5), 3.82 (1H, d, J = 3.2 F-3), 3.79 (1H, t, J = 9.2 Hz, M-4), 3.78–3.82 (1H, m, M-6), 3.74–3.78 (1H, m, M-6), 3.72–3.76 (1H, m, M-5), 3.64 (7H, dd, J = 9.2, 3.3 Hz, G-2, G′-2), 3.57 (7H, t, J = 9.3 Hz, G-4, G′-4), 1.20 (3H, d, J = 6.6 Hz, F-6); ^{13}C NMR (125 MHz, D_2O) δ: 102.68–102.59 (7C, G-1, G′-1), 100.93 (1C, M-1), 96.69 (1C, F-1), 82.31–81.88 (7C, G-4, G′-4), 76.90 (1C, M-3), 73.92–73.69 (7C, G-3, G′-3), 73.58 (1C, M-5), 72.92–72.56 (13C, G-2, G′-2, G-5), 72.72–72.56 (1C, F-4), 71.27 (1C, G′-5), 70.37 (1C, F-3), 68.81 (1C, F-2), 67.56 (1C, F-5), 67.52 (1C, G′-6), 67.47 (1C, M-2),65.69 (1C, M-4), 61.73 (1C, M-6), 61.14–61.00 (6C, G-6), 16.11 (1C, F-6); HRFAB-MS Calcd for $C_{54}H_{89}O_{44}$ (M−H): 1441.4727. Found: 1441.4719.

3.3. Biological assay

3.3.1. Lectin blot analysis

HCT116 cells were treated with 6^{I},6^{IV}-di-*O*-[α-L-Fuc-(1→3)-α-D-Man]-βCD (**8**), 6-*O*-[α-L-Fuc-(1→3)-α-D-Man]-βCD (**9**), 6^{I},6^{IV}-di-*O*-(α-L-Fuc)-βCD (**10**), 6-*O*-(α-L-Fuc)-βCD (**11**), α-L-Fuc, α-L-Fuc-Man and βCD. After 72 h, the cells were harvested. The cells were precipitated by centrifugation at 2000 rpm for 5 min at 4 °C and then suspended in TNE buffer (10 mM Tris–HCl (pH 7.8), 1% NP40, 0.15 M NaCl, 1 mM ethylenediaminetetraacetic acid (EDTA)) containing a protease inhibitor cocktail (Roche, Basel, Switzerland). The suspension was placed on ice for 30 min to allow for solubilisation. The samples were then centrifuged at 15,000 rpm for 15 min at 4 °C, and the supernatants were collected. The cell lysates were quantitated using a Bicinchoninic Acid kit (BCA kit, Pierce, Rockford, IL). Cell lysates were subjected to SDS–PAGE under reducing conditions. One gel was subjected to Coomassie Brilliant Blue R-250 staining, and the other was transferred to a PVDF membrane for lectin blot analysis with fucose-binding lectin *Aleuria aurantia* lectin (AAL). AAL interacts with fucosylated oligosaccharides (Yamashita et al. 1985). After blocking with PBS containing 3% BSA overnight at 4 °C, the membrane was incubated in diluted biotinylated AAL (Seikagaku Corp., Tokyo, Japan) for 20 min at rt. It was then washed three times with TBST and incubated with dilute avidin-peroxidase conjugates (ABC kit, Vector Res. Corp., Burlingame, CA) for 20 min at rt. The membrane was again washed three times with TBST and developed using an ECL system.

3.3.2. Cell growth assay

The cells were seeded onto 96-well plates at 2500 cells/well. After 24 h, the fucosyl-βCDs (**8–11**) were added, and the cells were cultured for 72 h. The cells were then treated with a WST-8 solution (nacalai tesque) for 4 h. WST is a highly water-soluble disulfonated tetrazolium salt. Finally, the absorbance of the formazan products formed was detected at 450 nm.

3.3.3. Expression of α-L-fucosidase in HCT116

The HCT116 cells were treated with the fucosyl-βCDs (**8–11**), L-Fuc, Fuc-Man and βCD. After 72 h, the cells were harvested. The cell medium was removed, and the cells were collected with a cell scraper; then 500 μL of Trizol (Invitrogen, Carlsbad, CA) was added to the cultured cells. After 10 min, 100 μL of $CHCl_3$ was added, and the mixture was vortexed for 15 s and allowed to stand for 5 min. The tubes were centrifuged at 15,000 rpm at 4 °C for 15 min. The upper layer of each tube was moved to a new tube and an equal volume of 2-propanol was added; the mixture was vortexed and allowed to stand for 10 min. The tubes were then centrifuged at 15,000 rpm at 4 °C for 10 min. The upper layers were again removed, 70% ethanol was added to the precipitate, and the tubes were centrifuged at 15,000 rpm at 4 °C for 3 min. The upper layers were removed after standing for a few minutes. The precipitates were dissolved in 30 μL of diethylpyrocarbonate (DEPC)-treated H_2O. Then, 1 μg of RNA was mixed with an oligo dT primer and incubated at 70 °C for 10 min, immediately followed by incubation at 4 °C for 5 min. Ten microlitres of 5× buffer, 10 μL of dNTP, 5 μL of 0.1 M DTT and 13 μL of DEPC water were added, and the mixture was incubated at 42 °C for 2 min. Then, 1 μL of super script rt was added over ice, and the mixture was incubated at 42 °C for 40 min, 95 °C for 5 min and 4 °C for 5 min. Then, 1 μL of RNase (10 mg/ml) was added, and the mixture incubated at 37 °C for 20 min. Each synthesised cDNA was diluted ten-fold. Two microlitres of each diluted cDNA was adjusted to a 20 μL solution containing Taq polymerase and 0.4 μM forward and reverse primers. After initial polymerase activation and a denaturation step of 2 min at 94 °C, the samples underwent 20 amplification cycles, each comprising 15 s at 94 °C, 30 s at 62 °C, and 1 min at 68 °C. PCR products were subjected agarose electrophoresis and visualised with ethidium bromide. The primer sequences for hFUCA1 (human α-fucosidase 1), hFUCA2, and glyceraldehyde-3-phosphate dehydrogenase (GAPDH) were as follows:

FUCA1: Forward primer: 5′-CACTGGCCAGAAAATGGAGTCTT-3′,
Reverse primer: 5′-TGAAGCAGGAAAACAGTGAGCAG-3′;
FUCA2: Forward primer: 5′-GGCACAGTAGTCACCAATGATCG-3′,
Reverse primer: 5′-GTGGGCCCAATATTCATCAAAAG-3′;
GAPDH: Forward primer: 5′-AACGGGAAGCTTGTCATCAAT-3′,
Reverse primer: 5′-GCCAGTGAGCTTCCCGTTCA-3′. GAPDH was used as an internal control.

Acknowledgement

We thank the Shin Nihon Chemical Co., Ltd (Aichi, Japan) for supplying the α-fucosidase (Sumizyme PHY).

References

1. Shinoda, T.; Kagatani, S.; Maeda, A.; Konno, Y.; Hashimoto, H.; Hara, K.; Fujita, K.; Sonobe, T. *Drug Dev. Ind. Pharm.* **1999**, *25*, 1185–1192.
2. Hattori, K.; Kenmoku, A.; Mizuguchi, T.; Ikeda, D.; Mizuno, M.; Inazu, T. *J. Inclusion Phenom. Macrocyclic Chem.* **2006**, *56*, 9–16.
3. Oda, Y.; Yanagisawa, H.; Maruyama, M.; Hattori, K.; Yamanoi, T. *Bioorg. Med. Chem.* **2008**, *16*, 8830–8840.
4. French, D. *Adv. Carbohydr. Chem.* **1957**, *12*, 189–260.
5. Ikuta, A.; Mizuta, N.; Kitahata, S.; Murata, T.; Usui, T.; Koizumi, K.; Tanimoto, T. *Chem. Pharm. Bull.* **2004**, *52*, 51–56.
6. Ikuta, A.; Koizumi, K.; Tanimoto, T. *J. Carbohydr. Chem.* **2003**, *22*, 297–308.
7. Tanimoto, T.; Kishimoto, Y.; Ikuta, A.; Nishi, Y.; Miyake, K. *J. Inclusion Phenom. Macrocyclic Chem.* **2002**, *44*, 297–302.
8. Ikuta, A.; Koizumi, K.; Tanimoto, T. *J. Carbohydr. Chem.* **2000**, *19*, 13–23.
9. Tanimoto, T.; Sakaki, T.; Koizumi, K. *Carbohydr. Res.* **1995**, *267*, 27–37.
10. Tanimoto, T.; Omatsu, M.; Ikuta, A.; Nishi, Y.; Murakami, H.; Nakano, H.; Kitahata, S. *Biosci. Biotechnol. Biochem.* **2005**, *69*, 732–739.
11. Kitahata, S.; Tanimoto, T.; Okada, Y.; Ikuta, A.; Tanaka, K.; Murakami, H.; Nakano, H.; Koizumi, K. *Biosci. Biotechnol. Biochem.* **2000**, *64*, 2406–2411.
12. Kitahata, S.; Tanimoto, T.; Ikuta, A.; Tanaka, K.; Fujita, K.; Hashimoto, H.; Murakami, H.; Nakano, H.; Koizumi, K. *Biosci. Biotechnol. Biochem.* **2000**, *64*, 1223–1229.
13. Hamayasu, K.; Hara, K.; Fujita, K.; Kondo, Y.; Hashimoto, H.; Tanimoto, T.; Koizumi, K.; Nakano, H.; Kitahata, S. *Biosci. Biotechnol. Biochem.* **1997**, *61*, 825–829.
14. Koizumi, K.; Tanimoto, T.; Okada, Y.; Hara, K.; Fujita, K.; Hashimoto, H.; Kitahata, S. *Carbohydr. Res.* **1995**, *278*, 129–142.
15. Townsend, R. R.; Hardy, M. R.; Wong, T. C.; Lee, Y. C. *Biochemistry* **1986**, *25*, 5716–5725.
16. Lee, Y. C.; Lee, R. T. *Acc. Chem. Res.* **1995**, *28*, 321–327.
17. French, D.; Levine, M. L.; Pazur, J. H.; Norberg, E. *J. Am. Chem. Soc.* **1949**, *71*, 353–356.
18. Okada, Y.; Matsuda, K.; Hara, K.; Hamayasu, K.; Hashimoto, H.; Koizumi, K. *Chem. Pharm. Bull.* **1999**, *47*, 1564–1568.
19. Hakomori, S. *Prog. Biochem. Pharmacol.* **1975**, *10*, 167–196.
20. Hakomori, S. *Annu. Rev. Biochem.* **1981**, *50*, 733–764.
21. Hakomori, S. *Cancer Res.* **1985**, *45*, 2405–2414.

22. Moriwaki, K.; Noda, K.; Fukukawa, Y.; Ohshita, K.; Uchiyama, A.; Nakagawa, T.; Taniguchi, N.; Daigo, Y.; Nakamura, Y.; Hayashi, N.; Miyoshi, E. *Gastroenterology* **2009**, *137*, 188–198.
23. Nishi, Y.; Tanimoto, T. *Biosci. Biotechnol. Biochem.* **2009**, *73*, 562–569.
24. Ikuta, A.; Tanimoto, T.; Koizumi, K. *Carbohydr. Res.* **2003**, *22*, 297–308.
25. Ajisaka, K.; Fujimoto, H.; Miyasato, M. *Carbohydr. Res.* **1998**, *309*, 125–129.
26. Murata, T.; Morimoto, S.; Zeng, X.; Watanabe, S.; Usui, T. *Carbohydr. Res.* **1999**, *320*, 192–199.
27. Koizumi, K.; Okada, Y.; Nakanishi, N.; Tanimoto, T.; Takagi, Y.; Ishikawa, M.; Ishigami, H.; Hara, K.; Hashimoto, H. *J. Carbohydr. Chem.* **1991**, *10*, 657–670.
28. Sugimoto, M.; Numata, M.; Koike, K.; Nakahara, Y.; Ogawa, T. *Carbohydr. Res.* **1987**, *163*, 209–225.
29. Doddrell, D. M.; Pegg, D. T. *J. Am. Chem. Soc.* **1980**, *102*, 6388–6390.
30. Koizumi, K.; Tanimoto, T.; Okada, Y.; Takeyama, S.; Hamayasu, K.; Hashimoto, H.; Kitahata, S. *Carbohydr. Res.* **1998**, *314*, 115–125.
31. Wang, X.; Gu, J.; Ihara, H.; Miyoshi, E.; Honke, K.; Taniguchi, N. *J. Biol. Chem.* **2006**, *281*, 2572–2577.
32. Rosenbaum, A. I.; Zhang, G.; Warren, J. D.; Maxfield, F. R. *Proc. Natl. Acad. Sci.* **2010**, *107*, 5477–5482.
33. Koizumi, K.; Tanimoto, T.; Fujita, K.; Hara, K.; Kuwahara, N.; Kitahata, N. *Carbohydr. Res.* **1993**, *238*, 75–91.

J Gastroenterol
DOI 10.1007/s00535-013-0813-2

ORIGINAL ARTICLE—LIVER, PANCREAS, AND BILIARY TRACT

Expression of *N*-acetylglucosaminyltransferase V in the subserosal layer correlates with postsurgical survival of pathological tumor stage 2 carcinoma of the gallbladder

Kenichiro Onuki · Hiroaki Sugiyama · Kazunori Ishige · Toru Kawamoto · Takehiro Ota · Shunichi Ariizumi · Masayuki Yamato · Shinichi Kadota · Kaoru Takeuchi · Akiko Ishikawa · Masafumi Onodera · Kojiro Onizawa · Masakazu Yamamoto · Eiji Miyoshi · Junichi Shoda

Received: 15 January 2013 / Accepted: 1 April 2013

Abstract
Background *N*-Acetylglucosaminyltransferase V (GnT-V), an enzyme that catalyzes the β1-6 branching of *N*-acetylglucosamine on asparagine-linked oligosaccharides of cellular proteins, enhances the malignant behaviors of carcinoma cells in experimental models. The aim of this study was to determine clinical significance of GnT-V expression in human pT_2 gallbladder carcinoma with simple in vitro experiments.
Methods Ninety patients with pT_2 gallbladder carcinoma were included for this study. The in vitro and in vivo biological effects of GnT-V were investigated using gallbladder carcinoma cells with variable GnT-V expression levels induced by a small interfering RNA.
Results Of the 90 cases, 57 showed positive staining and the remaining 33 demonstrated negative staining, the subcellular localization in the 57 cases was classified into the granular-type in 31 cases and the diffuse-type in 26 cases. In 76 cases with curative resection, postsurgical survival was significantly poorer in those showing positive staining than in those showing negative staining ($P = 0.028$). In all of the 76 cases, postsurgical recurrence was significantly more frequent in those showing diffuse-type localization than in those showing negative staining. Experimental analyses demonstrated that the down-regulation of GnT-V expression in gallbladder carcinoma cells induced suppression of cell growth in vitro. The expression levels of GnT-V in the cells were highly correlated with the rapid in vivo growth coupled with the enhanced angiogenesis, and the tendency to form liver metastasis.
Conclusions GnT-V expression in the subserosal layer of pT_2 gallbladder carcinoma is correlated with the aggressiveness of the disease.

K. Onuki · T. Kawamoto · T. Ota · S. Ariizumi · M. Yamamoto
Department of Surgery, Institute of Gastroenterology, Tokyo Women's Medical University, Shinjuku-ku, Tokyo, Japan

H. Sugiyama · K. Ishige
Department of Gastroenterology, Division of Biomedical Science, Faculty of Medicine, University of Tsukuba, Tsukuba, Ibaraki, Japan

M. Yamato
Institute of Advanced Biomedical Engineering and Science, Tokyo Women's Medical University, Shinjuku-ku, Tokyo, Japan

S. Kadota · K. Takeuchi
Department of Infection Biology, Division of Biomedical Science, Faculty of Medicine, University of Tsukuba, Tsukuba, Ibaraki, Japan

A. Ishikawa · E. Miyoshi
Division of Health Sciences, Osaka University Graduate School of Medicine, Suita, Osaka, Japan

M. Onodera
Department of Genetics, National Research Institute for Child Health and Development, Setagaya-ku, Tokyo, Japan

K. Onizawa
Department of Oral and Maxillofacial Surgery, Division of Biomedical Science, Faculty of Medicine, University of Tsukuba, Tsukuba, Ibaraki, Japan

J. Shoda (✉)
Medical Science, Division of Clinical Science, Faculty of Medicine, University of Tsukuba, Tsukuba, Ibaraki 305-8575, Japan
e-mail: shodaj@md.tsukuba.ac.jp

Published online: 17 April 2013

Keywords Gallbladder carcinoma · *N*-Acetylglucosaminyltransferase V · Malignant behavior · Postsurgical prognosis · Tumor cell biology

Abbreviations

mAb	Monoclonal antibody
GalNAc-T	*N*-acetylgalactosaminyltransferase
GnT-V	*N*-acetylglucosaminyltransferase
pT	Pathological tumor stage

Introduction

Gallbladder carcinoma has always been associated with a dismal overall prognosis, and this is because the disease is usually detected at an advanced stage [1–5]. The clinical course of gallbladder carcinoma has been thought to depend on the depth of tumor invasion. The 5-year postsurgical survival rates were decreased with tumor invasion: 86–100 % for pathological tumor stage 1 (pT_1) carcinoma, 56–85 % for pT_2 carcinoma, 40–57 % for pT_3 carcinoma, and 9–19 % pT_4 carcinoma [6–8]. Despite a theoretical advantage for pT_2 gallbladder carcinoma (a tumor invading the perimuscular connective tissues but not extending beyond the serosa or into the liver), the prognosis of the disease is not necessarily favorable. The parameters of histopathological malignancies such as lymphatic permeation and venous permeation in the subserosal layer are not correlated with either the mode of recurrence or postsurgical prognosis of pT_2 gallbladder carcinoma [9]. These findings are attributed to various mechanisms in which pT_2 gallbladder carcinoma progresses and to the fact that prognostic factors affecting the progression of less-advanced lesions such as pT_2 gallbladder carcinoma have not been fully elucidated.

Recent advances in glycomics have revealed the scope and scale of the functional roles of oligosaccharides and their effect on human diseases [10]. It is a well-known fact that oligosaccharide structures are dramatically changed in carcinogenesis including malignant transformation. Oligosaccharides are synthesized by a set of several glycosyltransferases, whose genes are approximately 1 % of the human genome. *N*-Acetylglucosaminyltransferase V (GnT-V) is one of the most important among several kinds of glycosyltransferases, which are enzymes involved in carcinogenesis and tumor metastasis [11–13]. GnT-V is involved in the synthesis of β1-6 GlcNAc branching formation on *N*-glycans. A study of GnT-V-deficient mice clearly showed that GnT-V was essential for tumor growth and metastasis [14]. The mechanisms underlying how GnT-V regulates tumor metastasis involve the up-regulation of signaling of many growth factor receptors on the cell surface by suppressing their endocytosis [15], the enhancement of certain kinds of protease activity [16], and the stimulation of angiogenesis as a co-factor [17]. However, immunohistochemical studies of GnT-V showed that GnT-V expression is correlated with poor prognosis of certain kinds of cancer [18, 19], but inversely correlated with other types of cancers [20, 21]. This discrepancy might be dependent on whether or not cancer cells have target proteins of GnT-V or a protease involved in GnT-V cleavage. Although GnT-V has been shown to induce tumor angiogenesis by at least 2 different pathways [16, 17] as well as growth of tumor cells through the up-regulation of growth factor receptors [15], combination studies of clinical and experimental aspects have not yet been performed. Furthermore, pathological investigation of GnT-V products showed that aberrant localization of glycoproteins bearing β1-6 GlcNAc branching is a sign of poor prognosis in melanoma cells [22].

In this retrospective analysis, the immunohistochemical expression of GnT-V was investigated in formalin-fixed, paraffin-embedded surgical specimens from patients with pT_2 gallbladder carcinoma. In 90 cases of pT_2 gallbladder carcinoma, correlations of GnT-V immunostaining at the deepest invading sites in the subserosal layer, as a predictor of invasive/metastatic potential, with the clinicopathological findings, mode of recurrence, and postsurgical survival were investigated. Furthermore, the biological effects of GnT-V on in vitro and in vivo models were studied using gallbladder carcinoma cells with variable GnT-V expression levels induced by a small interfering RNA (siRNA).

Materials and methods

Patients

Specimens from 186 patients (20 normal gallbladder, 19 gallbladder stones, 17 pT_1 gallbladder carcinoma, 90 pT_2 gallbladder carcinoma, 20 pT_3 gallbladder carcinoma and 20 pT_4 gallbladder carcinoma) were included in this study. In the 90 patients with pT_2 gallbladder carcinoma (40 men and 50 women), 76 were curatively resected with a free surgical margin. The mean age of the patients was 67 years (range, 36–83 years). The patients were diagnosed as having gallbladder carcinoma and underwent surgery between 1983 and 2008 in the Department of Surgery, Institute of Gastroenterology, Tokyo Women's Medical University Hospital. Gallbladder carcinoma was diagnosed on the basis of histological findings and classified according to the Tumor-Node-Metastasis classification of the American Joint Committee on Cancer [23]. According to the institutional surgical treatment strategy for pT_2 gallbladder carcinoma, simple cholecystectomy was performed

in 50 patients, cholecystectomy combined with bile duct resection in 9 patients, cholecystectomy combined with bile duct resection and hepatic resection in 12 patients, cholecystectomy combined with bile duct resection and pancreatoduodenectomy in 10 patients, and cholecystectomy combined with pancreatoduodenectomy together with bile duct resection and hepatic resection in 9 patients. Histological examination revealed that all cases of pT_2 gallbladder carcinoma had neither hepatic infiltration nor invasion into the hepatoduodenal ligament.

The follow-up periods until February 2008 ranged from 2.3 to 241.9 months (median time 64 months). Of the 76 patients who had undergone the curative resection with a free surgical margin, 60 were alive as of May 2008, 13 had died from peritoneal dissemination, distant organ metastasis, lymph nodes metastasis and/or local recurrence, and 3 had died from other diseases (cerebral infarction in 1, pseudomixoma in 1, and pneumonia in 1). The latter 3 patients were treated as lost cases.

Cell lines and culture conditions

The gallbladder carcinoma cell lines Mz-ChA-1 and Mz-ChA-2 [24] were obtained from Dr. Alexander Kruth (Johaness-Gutenberg University, Mainz, Germany). The gallbladder carcinoma cell lines TGBC-1-TKB, TGBC-2-TKB, and TGBC-44-TKB (TG44) [25] were obtained from Dr. Takeshi Todoroki (University of Tsukuba, Ibaraki, Japan). The cells were maintained in Dulbecco's modified Eagle's medium containing 10 % heat-inactivated fetal calf serum (Hyclone Laboratories Inc., Logan, UT, USA) in a humidified atmosphere with 5 % carbon dioxide at 37 °C.

Immunoblot analysis of GnT-V

Immunoblot analysis of GnT-V was performed using the lysates of either frozen tissue specimens or cultured cells as described previously [26]. In brief, after 20–30 μg of proteins were electrophoresed on 10 % SDS-PAGE, and then transferred onto a polyvinylidine difluoride (PVDF) membrane. The membranes were incubated overnight in 2 % bovine serum albumin (BSA) in phosphate buffered saline (PBS) at 4 °C and then mixed with a mAb against GnT-V 24D11 (Fuji-revio, Tokyo, Japan) diluted in 2 % BSA (1:500) for 2 h. Each membrane was again probed with a mAb against β-actin (Sigma-Aldrich Co., St. Louis, MO, USA) diluted in 2 % BSA (1:1000). After washing with PBS, the membranes were incubated with goat anti-rabbit or anti-mouse IgG labeled with horseradish peroxidase (Zymed Laboratories Inc., San Francisco, CA, USA) for 40 min. The membranes were then washed with PBS and treated using enhanced chemiluminescence (ECL) (Amersham, Buckinghamshire, UK) to visualize bound antibodies.

Lectin blot analysis

For lectin blot analysis, the membranes were blocked with 3 % BSA in TBST, followed by incubation with 10 μg/ml biotinylated L_4-PHA lectin (Seikagaku Corp., Tokyo, Japan). Reactive bands were detected using the ECL system.

Immunostaining of GnT-V and CD31

Gallbladder carcinoma tissues that had been preserved in 10 % formalin and then embedded in paraffin were serially sectioned at 2 μm thickness, mounted on silane-coated slides, and deparaffinized. The slides were immersed for 20 min in 0.3 % hydrogen peroxide in methanol to deplete endogenous peroxidase. After washing with PBS, the slides were incubated with a protein blocking agent for 5 min at room temperature in a humidity chamber. The slides were then stained by the indirect immunoperoxidase method using an anti-GnT-V antibody, 22G12 (Fuji-revio, Tokyo, Japan) at a 1:3000 dilution rate. A negative control was made using BSA instead of the mAb. Detail procedure was described previously [18].

Evaluation of sections was performed by a single pathologist who was blinded to the clinical characteristics and pathological grade of response. The total number of cancerous epithelia in each section was evaluated. The immunohistochemical localization of GnT-V was classified into the granular-type and diffuse-type based on the predominant subcellular distribution: the granular-type was defined as GnT-V showing granular staining and being restricted predominantly in the supranuclear area of the cancerous epithelia; the diffuse-type was defined as GnT-V showing no granular staining and being found in the cytoplasm of the cancerous epithelia. GnT-V localization was judged to be either the granular or diffuse type when 50 % of the total number of cancerous epithelia in each section showed granular-type or diffuse-type subcellular distribution, and the localization was examined in both the mucosal or proper muscle layers (surface site) and the subserosal layer (invading site).

To investigate the association of GnT-V expression with tumor angiogenesis in gallbladder carcinoma, microvessels (capillaries and venules) around the cancerous epithelia were counted. Microvessels were highlighted by staining the endothelial cells with mAb raised against CD31 (Abcam, Cambridge, MA, USA) according to the standard immunoperoxidase technique [27]. Areas representative of the invasive component of the carcinoma were selected from the hematoxylin and eosin-stained sections. Microvessel density was assessed without prior knowledge of GnT-V staining. Microvessels were carefully counted (per 100× field) and the microvessel density in each field was

defined as the mean number of microvessels containing high levels of CD31-stained microvessels.

Construction of GnT-V knockdown gallbladder carcinoma cells

Suppression of GnT-V expression in TG44 cells was achieved using a siRNA duplex. A retrovirus, which encodes a siRNA against GnT-V, was obtained from Dr. Naoyuki Taniguchi [28]. TG44 cells were infected with the retrovirus, and then the cells were selected with 0.8 mg/ml G418 for 2–3 weeks. Stable GnT-V knockdown TG44 cells were cloned and confirmed by immunoblot analysis as described earlier.

Construction of gallbladder carcinoma cells expressing luciferase

To establish TG44 cells expressing luciferase (TG44-luc), TG44 cells were infected with a retrovirus encoding luciferase and enhanced green fluorescent protein (EGFP), which was generated by Dr. Masafumi Onodera [29, 30], and the resulting cells were cultured for 3–7 days. Cell lysates were prepared and subjected to luciferase assay (Promega, Madison, WI) to confirm luciferase expression.

Enzyme assay of GnT-V

GnT-V enzyme activity was determined as described previously [31].

Cell viability assay

The in vitro effects of GnT-V on the growth viability of gallbladder carcinoma cells were determined by a cell viability assay using a WST-8 reduction assay kit (Dojin Laboratories, Tokyo, Japan) according to the manufacturer's instructions. Gallbladder carcinoma cells were plated at 1×10^3 cells per well in 96-well microtiter plates. WST-8 was added and cell viability was determined by reading optical density values from a microplate reader at an absorption wavelength of 450 nm. All assays were performed twice. The IC_{50} value, at which 50 % cell growth inhibition compared with that of the dimethyl sulfoxide control was obtained, was calculated.

Subcutaneous xenografted tumor model

Four-week-old female BALB/c nu/nu athymic mice (Sankyo Labo Service, Tokyo, Japan) were quarantined for 1 week. The animal experiment protocols were approved by the Institutional Animal Care and Use Committee of Tokyo Women's Medical University. A gallbladder carcinoma xenograft model was prepared by injecting 1×10^7 TG44 cells induced by a siRNA in 100 μl of PBS into the left flank of each mouse. Tumor size was measured using a Vernier caliper and tumor volume was calculated as 0.5 × longest diameter × width^2.

Persplenic hepatometastatic tumor model

A persplenic hepatometastatic tumor model injected with 2×10^6 TG44-luc cells induced by a siRNA was prepared as previously described [32]. In the mice, photon counting was conducted once a week. Bioluminescence images were used to monitor the dynamics of intrahepatic tumor growth. Immediately before imaging, 150 mg/kg D-luciferin (Alameda, CA, USA) was intraperitoneally administered to the mice. After 15 min, photons from whole bodies were counted using the IVIS imaging system (Xenogen, CA, USA) in accordance with the manufacturer's instructions. Total flux (photons/sec) of emitted light was used as a measure of the relative number of viable tumor cells in the peritoneal tumor. Data were analyzed using LIVING IMAGE 3.0 software (Xenogen).

Statistical analysis

Values are presented as mean ± SE (standard error). Statistical evaluations of data were analyzed using the χ^2 test for independence test, Student's *t* test, and one-way ANOVA followed by the Tukey–Kramer test. Survival curves of the postsurgical outcome of the 76 curative resection cases of pT_2 gallbladder carcinoma and animals in the hepatometastatic tumor model were analyzed using the Kaplan–Meier method. Differences in the survival of the 76 curative resection cases of pT_2 gallbladder carcinoma and animals in the subgroups were analyzed by the log-rank test. Several clinicopathological factors were subjected to multivariate regression analysis using the Cox proportional hazards regression model. Cox regression was accessed using the statistical program SPSS. A *P* value of less than 0.05 was considered to indicate a statistically significant difference.

Results

Immunoblot analysis of GnT-V in gallbladder carcinoma tissues

GnT-V protein was included in the lysates of the specimens of gallbladder carcinomas and normal gallbladders (Fig. 1a). GnT-V protein levels were increased at varying degrees in the tissue specimens of pT_1–pT_3 gallbladder carcinomas compared with the GnT-V protein levels in the specimens of normal gallbladders (Fig. 1a).

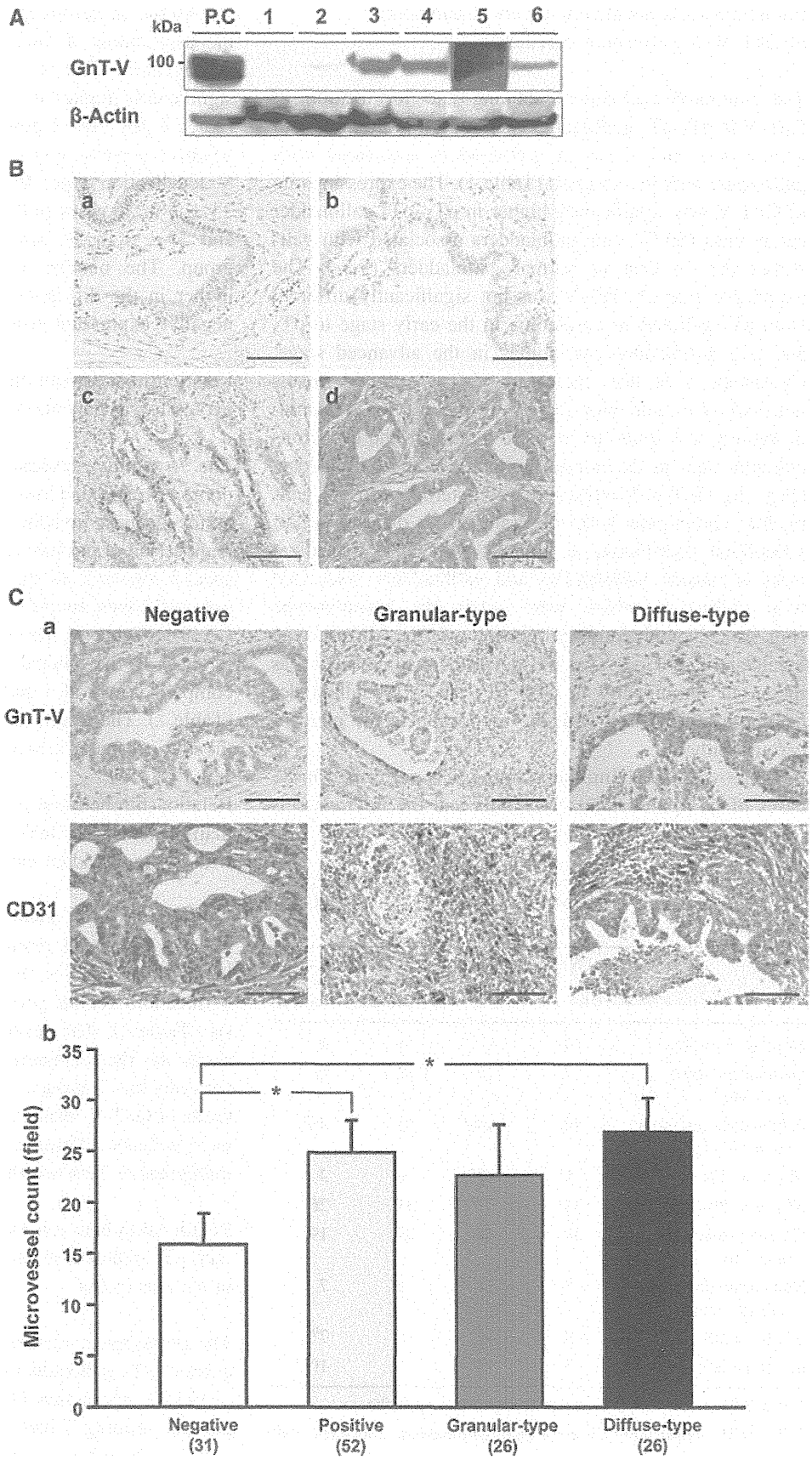

Fig. 1 A Immunoblot analysis of GnT-V in normal gallbladders and gallbladder carcinoma tissues. Protein was normalized to β-actin. GnT-V transfected WiDr cells (a colon carcinoma cell line) was used as a positive control (P.C). *Lanes 1* and *2* lysates of normal gallbladders, *Lane 3* lysate of pT_1 gallbladder carcinoma tissue, *Lanes 4* and *5* lysates of pT_2 gallbladder carcinoma tissues, *Lane 6* lysate of pT_3 gallbladder carcinoma tissue. **B** Immunohistochemical localization of GnT-V in the epithelia of normal gallbladder (**a**), in those of gallbladder associated with gallstones (**b**), and those of pT_2 gallbladder carcinoma (**c**, **d**). GnT-V localization was mostly the granular-type for normal epithelia and noncancerous pathological epithelia of the gallbladders. However, GnT-V localization was heterogeneous: granular- (**c**) and diffuse- (**d**) types for the cancerous epithelia of gallbladder carcinoma. *Bars* 100 μm. **C** Immunostainings of CD31 and GnT-V in the epithelia of pT_2 gallbladder carcinoma. *Bars* 100 μm (**a**). Quantification of data of microvessel density in tissue sections. A tissue section was prepared from each case of gallbladder carcinoma patients. Five photographs were taken for each tissue section and analyzed. Microvessels showing CD31 immunoreactivity was counted. Microvessel density for each of the 5 photographs of the tissue section was averaged. The averaged densities were compared in terms of GnT-V expression levels (**b**). *Columns* and *bars* represent means and SE of the microvessel densities in each group, respectively. Significant differences between the 2 groups are indicated by $^*P < 0.05$

Immunohistochemical staining and localization of GnT-V in gallbladder carcinoma

The immunohistochemical staining and localization of GnT-V in pT_1-pT_4 gallbladder carcinomas, those in normal gallbladders and those in gallbladders associated with gallstones, were investigated (Table 1). The expression rate of GnT-V was significantly higher in pT_1–pT_4 gallbladder carcinomas (69 %) and gallbladders associated with gallstones (63 %) than in normal gallbladders (5 %). The expression rate of GnT-V was not significantly different from pT_1 gallbladder carcinoma in the early stage to pT_3 and pT_4 gallbladder carcinomas in the advanced stage. Consistent with the increased GnT-V protein levels detected by immunoblot analysis (Fig. 1a), GnT-V immunostaining was found to be more intense in the cancerous epithelia than in the normal epithelia of the gallbladders (Fig. 1b). GnT-V localization was heterogeneous in gallbladder carcinomas with the granular- or diffuse-type of subcellular distribution, in contrast with GnT-V localizations in normal gallbladders and gallbladders associated with gallstones, which were solely the granular-type (Fig. 1b). Notably, the proportion of the diffuse-type localization of GnT-V at the deepest invading sites was increased significantly in pT_2, pT_3, and pT_4 gallbladder carcinomas compared with the proportion in the noncancerous epithelia.

Moreover, CD31 immunostaining was performed in 83 cases of pT_2 gallbladder carcinoma and the microvessels around the cancerous epithelia were counted to investigate the association of GnT-V expression levels with tumor angiogenesis (Fig. 1c). The number of microvessels was significantly higher in 52 cases with positive expression (25 ± 3 per 100 × power field) than in 31 cases with negative expression (16 ± 3). Moreover, in terms of GnT-V localization type, the numbers of microvessels were 23 ± 5 in 26 cases in the granular-type locatization group and 27 ± 3 in 26 cases in the diffuse-type localization group. The number of microvessels was significantly higher in the diffuse-type localization group than in the negative expression group.

Table 1 The immunohistochemical localization of GnT-V in normal epithelia and that in gallbladder stones and pT_1–pT_4 gallbladder carcinomas

	Negative	Positive	Localization type	
			Granular	Diffuse
Normal ($n = 20$)	19	1	1	0
Gallbladder stone ($n = 19$)	7	12	12	0
Gallbladder carcinoma ($n = 147$) (pT_1–pT_4)	46	101[a]	55	46[b]
pT_1 ($n = 17$)	5	12[a]	9	3
pT_2 ($n = 90$)	33	57[a]	31	26[b]
Curative resection case ($n = 76$)	30	46	27	19
Non-curative resection case ($n = 14$)	3	11	4	7
pT_3 ($n = 20$)	3	17[a]	10	7[b]
pT_4 ($n = 20$)	5	15[a]	5	10[b,c]

[a] $P < 0.01$, significantly different from normal epithelia

[b] $P < 0.01$, significantly different from gallbladders associated with gallstones

[c] $P < 0.05$, significantly different from pT_1 carcinoma

Relationship between clinical findings and GnT-V expression in patients with pT_2 gallbladder carcinoma

The 76 curative resection cases of pT_2 gallbladder carcinoma were divided into 2 groups based on GnT-V staining at the deepest invading sites in the subserosal layer. A comparison of positive and negative groups was made with special reference to the clinical features, that is, gender, age, gallstones, tumor size, preoperative serum CEA, and CA19-9 (Table 2). The results revealed no significant differences in the clinical features between the 2 groups. A comparison was also made in terms of GnT-V localization (Table 2). The results showed no significant differences in the clinical features between the 2 groups.

Relationship between parameters of pathological malignancies and GnT-V expression in patients with pT_2 gallbladder carcinoma

A comparison of positive and negative groups was also made with special reference to the parameters of pathological malignancies, that is, histological grade, lymphatic permeation, venous permeation, and lymph node metastasis (Table 3). The results revealed no significant differences in the parameters of pathological malignancies between the 2 groups. A comparison was also made in terms of GnT-V localization (Table 3). The results showed no significant differences in the parameters of pathological malignancies between the 2 groups.

Relationship between mode of recurrence in patients with pT_2 gallbladder carcinoma and GnT-V expression in the specimens

The postsurgical recurrent mode in 76 curative resection cases of pT_2 gallbladder carcinoma was compared in terms of GnT-V expression (Table 4). Of the 46 cases showing positive staining, 7 had distant organs metastasis and 6 had lymph node metastasis. In contrast, of the 30 cases showing negative staining, 1 had peritoneal dissemination and 1 had

Table 2 Relationship between clinical findings and immunohistochemical expression of GnT-V in curative resection cases of pT2 gallbladder carcinoma

	Negative	Positive	Localization type	
			Granular	Diffuse
Number	30	46	27	19
Gender (M/F)	11/19	20/26	10/17	10/9
Age	65 ± 12	68.2 ± 9.8	67.6 ± 9	68.9 ± 10
Gallstones (±)	14/16	24/22	14/13	10/9
Tumor size (mm)	32.5 ± 18	32.1 ± 20.5	30.9 ± 18.7	33.5 ± 22.6
CEA	4.17 ± 8.2	4.37 ± 6.6	3.99 ± 6.77	4.65 ± 6.91
CA19-9	34.2 ± 49.3	414.9 ± 1228	686.7 ± 1640	29.1 ± 31.9

Table 3 Correlation between histopathological findings and immunohistochemical localization of GnT-V in pT_2 gallbladder carcinomas

	Negative	Positive	Localization type	
			Granular	Diffuse
Number	30	46	27	19
Histlogical grade				
G1	17	33	20	13
G2-4	13	13	7	6
Lymphatic permeation				
+	18	34	19	15
−	12	12	8	4
Venous permeation				
+	16	18	12	6
−	14	28	15	13
Lymph node metastasis				
+	11	19	10	9
−	19	27	17	10

There is no significant difference between immunohistochemical localization of GnT-V and histopathological findings of the 76 curative cases of pT_2 gallbladder carcinomas

distant organs metastasis. Note that in pT_2 gallbladder carcinoma, postsurgical recurrence in distant organs tended to be more frequent in patients in the positive staining group (15 %) than in patients in the negative staining group (3 %). Moreover, postsurgical recurrence in distant organs was found to be significantly more frequent in the diffuse-type localization group (26 %) than in the negative staining group (3 %; $P < 0.05$). Therefore, the diffuse-type localization of GnT-V at the deepest invading sites may be an important biological predictor of postsurgical recurrence of pT_2 gallbladder carcinoma.

Relationship between synchronous metastasis in the liver of patients with pT_2, pT_3 or pT_4 gallbladder carcinoma and GnT-V expression in the specimens

GnT-V expression at the deepest invading sites was compared in pT_2, pT_3 and pT_4 gallbladder carcinoma patients with synchronous liver metastasis at the time of surgery and those without metastasis (Table 5). Of 130 patients, 14 had synchronous liver metastasis and the remaining 116 had none. Synchronous liver metastasis was found to be significantly more frequent in the diffuse-type localization group (19 %) than in the negative staining group (5 %; $P < 0.05$).

Relationship between postsurgical survival of patients with pT_2 gallbladder carcinoma and GnT-V expression in the specimens

The overall postsurgical survival rate in the 76 patients with pT_2 gallbladder carcinoma was compared in terms of GnT-V expression (Fig. 2a). The survival rate of patients in the

Table 4 Postsurgical recurrent modes in pT_2 gallbladder carcinoma

Immunohistochemical localization of GnT-V	Total	Peritoneal dissemination	Distant organs[a]	Lymph Nodes	Local recurrence
Negative ($n = 30$)	5	1	1	0	3
Positive ($n = 46$)	16	0	7	6[d]	3
Granular-type ($n = 27$)	7	0	2	4	1
Diffuse-type ($n = 19$)	9[b]	0	5[c]	2	2

[a] Distant organs included the liver in 6 patients, lung in 1 patient and bone in 1 patient

[b] $P < 0.05$, significantly different from negative staining group

[c] $P < 0.05$, significantly different from negative staining group

[d] $P < 0.05$, significantly different from negative staining group

Table 5 Synchronous metastasis in the liver of patients with pT_2–pT_4 carcinomas and localization type of GnT-V in the specimens

	Total	Synchronous metastasis in the liver	No metastasis
pT_2–pT_4 carcinomas	130	14	116
Negative	41	2	39
Positive	89	12	77
Granular	46	4	42
Diffuse	43	8[a]	35

[a] $P < 0.05$, significantly different from negative staining group

positive staining group was significantly lower than that of patients in the negative staining group ($P = 0.028$). In addition, the survival rate of patients in the granular-type localization group and that of patients in the diffuse-type localization group tended to be lower, but not statistically significant, than that of patients in the negative staining group (Fig. 2b). A summary of the results of the multivariate regression analysis of prognostic factors for pT_2 gallbladder carcinoma is shown in Table 6. In the analysis, GnT-V was found to be a statistically significant independent risk factor compared with other clinicopathological factors.

Biological effects of GnT-V on gallbladder carcinoma cells in in vitro and in vivo tumor models

Cultured gallbladder carcinoma cells (e.g., Mz-ChA-1, TGBC-1-TKB, TGBC-2-TKB, and TGBC-44-TKB (TG44) cells) express high levels of GnT-V (data not shown). To investigate the biological effects of GnT-V on gallbladder carcinoma cells, a siRNA of GnT-V for suppressing GnT-V expression was introduced into TG44 cells using a retrovirus vector. As shown in Fig. 3a, variable suppression levels of GnT-V were observed in each of the established clones. Based on the protein level analysis, GnT-V activities, and lectin blot of PHA-L, 3 clones were selected for the in vitro and in vivo experiments. TG44-siR-H represented the highest values, whereas TG44-siR-L represented the lowest values. TG44-siR-M represented the intermediate values (Fig. 3a).

In vitro cell growth was fastest for the TG44-siR-H with higher GnT-V expression, the level of which is comparable to that of the original cells (Fig. 3a). On the other hand, in vitro cell growth was slow for the TG44-siR-L with lower GnT-V expression. The TG44-siR-M represented the intermediate growth speed. Similar to the in vitro growth, the TG44-siR-H represented rapid growth in the subcutaneous xenografted tumor model but TG44-siR-L represented slow growth (Fig. 3b). Histopathology, the subcutaneous tumor of TG44-siR-H yielded a high density of microvessels recognized by CD31 compared with those of TG44-siR-L and TG44-siR-M (Fig. 3b).

To mimic the clinical aggressiveness of gallbladder carcinoma cells with GnT-V expression, a persplenic hepatometastatic tumor model was developed using TG44-siR-H, TG44-siR-L, and TG44-siR-M cells. Seven days after persplenic injection of the cells, establishment of hepatometastasis was confirmed using the IVIS imaging

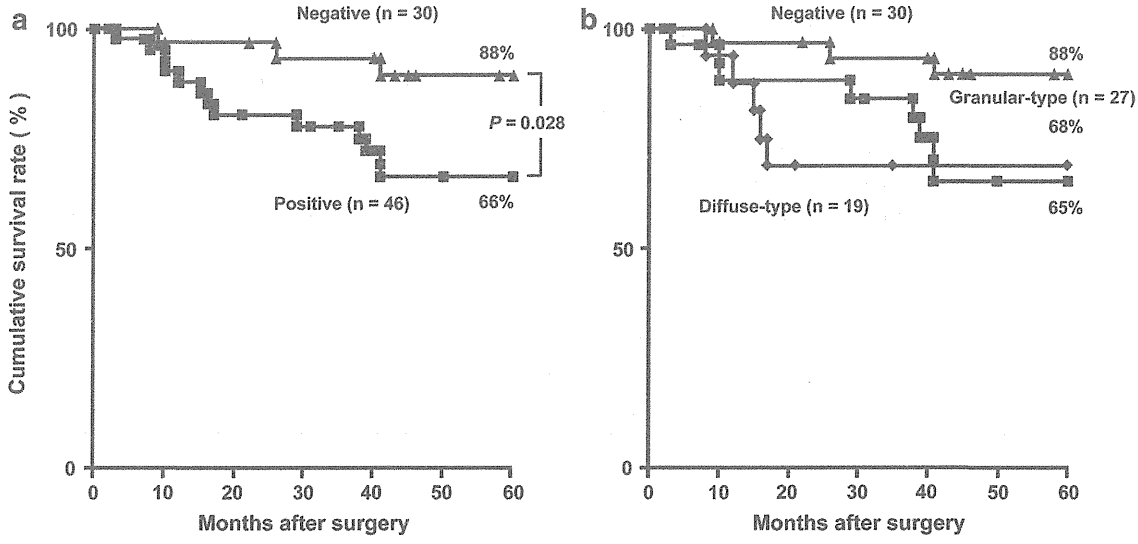

Fig. 2 **a** Relationships between postsurgical survival outcome and GnT-V expression status at the deepest invading sites in the surgical specimens of pT_2 gallbladder carcinoma as shown by Kaplan–Meier survival curves. The 76 curative resection cases of pT_2 gallbladder carcinoma were divided into 2 groups based on the GnT-V expression status ($P = 0.028$, log-rank test). **b** Relationship between postsurgical survival outcome and GnT-V localization-types. Cases showing positive staining were further divided into 2 groups based on the GnT-V localization types, that is, granular- and diffuse-type localization groups. However, there were no significant differences among the 3 groups

Table 6 Multivariate analysis of prognotic factors

Variable	Hazard ratio	C.L.	*P* value
GnT-V	4.82	1.1–21.2	0.038
N	0.82	0.2–8.4	0.780
Histological	2.53	0.7–9.1	0.155
Ly	1.62	0.3–7.9	0.548
Vy	0.45	0.1–1.7	0.244
Pn	0.98	0.2–4.2	0.982

system (Fig. 3c). Tumor volume in the intraperitoneal cavity was assessed using this imaging system which visualizes viable tumor cells as photon intensity (Fig. 3c). Regarding the time-course of change shown in Fig. 3c, the average photon intensity (total flux) was significantly increased in the mice bearing either TG44-siR-H or TG44-siR-M compared with that in the mice bearing TG44-siR-L. Correlating with the observed tumor aggressiveness, the survival period of the TG44-siR-H group (median survival period, 34 days) was significantly shorter than that of the TG44-siR-M group (median survival period, 60 days) and that of the TG44-siR-L group (all mice were alive at the end point of the observation period) (Fig. 3c).

Discussion

The major findings of this study are that the GnT-V protein levels were increased in the tissue specimens of gallbladder carcinoma compared with the GnT-V protein levels in the tissue specimens of normal gallbladder and that alteration in the subcellular localization of GnT-V is closely associated with the biological aspects of gallbladder carcinoma (e.g., aggressiveness to form distant organ metastasis).

The prognosis of pT_2 gallbladder carcinoma is not necessarily favorable despite a theoretical advantage for the carcinoma not invading the perimuscular connective tissues and not extending beyond the serosa or into the liver. This may be because approximately half of the patients had malignant infiltration into the lymphatic, venous, and perineural spaces, and the frequency of lymph node metastasis was 50 % [7, 33]. In this study, the diffuse-type localization of GnT-V at the deepest invading sites correlated with neither histological grade nor parameters of clinicopathological malignancies in the 76 curative resection cases of pT_2 gallbladder carcinoma. Because of the poor association of the expression level with the clinicopathological findings of pT_2 gallbladder carcinoma, the expression levels of GnT-V at the deepest invading sites may be considered to be an independent prognostic marker for pT_2 gallbladder carcinoma, as shown on the multivariate regression analysis (Table 6).

The regulatory basis for the diffuse-type localization on GnT-V immunohistochemistry of has not yet been well elucidated. The proportion of the diffuse-type localization was increased in parallel to the clinical stages of the disease (Table 1). Carcinoma cells at advanced stages are phenotypically different from their counterparts at early stages in their expression of mucin glycoproteins [34] and *N*-Acetylgalactosaminyltransferases (GalNAc-T family enzymes) [26]. Moreover, in relation to the presence of cytoplasmic or stromal localization of MUC1 mucin on immunohistochemistry, which was reported in the cases of pT_2 gallbladder carcinoma with high metastatic potential [9, 35], it has been hypothesized that mucin proteolysis takes place in vivo [36, 37]. A previous study has provided in vitro evidence that MUC1 mucin is cleaved by a metalloprotease(s) [38]. Metastatic gallbladder carcinoma cells may include cells with high levels of this kind of protease(s) mediating the GnT-V proteolysis. Taken together, these phenotypic changes affect the biological behavior of carcinoma cells with an increased metastatic potential.

It is also possible that alterations in the subcellular localization of GnT-V may be simply associated with the status of tumor differentiation and caused by loss of functional differentiation of the carcinoma cells, that is, the failure to establish or maintain the polar expression of normal epithelial localization of this enzyme. The diffuse-type localization of GnT-V in gallbladder carcinoma indicates a reorganization of the Golgi apparatus elements in the carcinoma cells as reported previously [39]. Therefore, the processing and targeting pathway of GnT-V may be defective in the cells. However, in cases of pT_2 gallbladder carcinoma, there was no strong correlation between histological grade (tumor differentiation), that is, papillary, tubular, or poorly differentiated adenocarcinoma, and the expression level of GnT-V at the deepest invading sites (Table 3), indicating that diffuse-type localization cannot be explained solely by differences in the histological grade of pT_2 carcinoma. Nevertheless, the expression level of GnT-V on immunohistochemistry may be a useful biological tool to scale the functional differentiation of pT_2 gallbladder carcinoma cells.

Malignant transformation of glandular epithelia is accompanied by alterations in the biochemical and biological characteristics of glycoproteins. In this study, the mechanism underlying the positive correlation between metastasis and GnT-V expression in pT_2 gallbladder carcinoma can be speculated on by the branching of asparagine-linked oligosaccharides, which is shown to regulate the metastatic potential of carcinoma cells [40]. The β1–6 branching structure, a product of GnT-V, is a good substrate for the attachment of poly-*N*-acetyllactosamine, whose synthesis is controlled by the complemental branch